Mfn2 induces NCLX-mediated Ca^{2+} release from mitochondria.

Authors: Panagiota Kolitsida[1], Akash Saha[1], Andrew Caliri[1], Essam Assali[2,3], Alejandro Martorell Riera[1,4], Samuel Itskanov[1,5], Sean Atamdede[6], Catalina S. Magana[1], Björn Stork[7], Orian Shirihai[8], Israel Sekler[2], Uri Manor[9], Carla M. Koehler[6] and Alexander M. van der Bliek[1]

Affiliations: [1]Department of Biological Chemistry, David Geffen School of Medicine at UCLA, [2]Department of Physiology and Cell Biology, Ben Gurion University, Israel, [3]Current: Yale School of Medicine, New haven CT, [4]Current: Kite Pharmaceutical, Santa Monica CA, [5]Current: Gilead Sciences, San Francisco CA , [6]Department of Chemistry and Biochemistry, UCLA, [7]Institute of Molecular Medicine I, Medical Faculty and University Hospital Düsseldorf, Heinrich Heine University Düsseldorf, Germany, [8]Department of Medicine, David Geffen School of Medicine at UCLA, [9]Department of Cell & Developmental Biology, School of Biological Sciences, University of California, San Diego. Correspondence to Alexander van der Bliek: avan@mednet.ucla.edu ORCID number 0000-0002-6211-5765 and Panagiota Kolitsida: p.kolitsida@gmail.com ORCID number 0000-0002-7330-1766; Mailing address: Department of Biological Chemistry, David Geffen School of Medicine, UCLA, 27-200N CHS, Los Angeles, California 90095-1737

Abstract

Mfn2 is a mitochondrial outer-membrane fusion protein that also functions as a tether between mitochondria and the ER. Here, we identify a previously unrecognized role for Mfn2 in regulating mitochondrial Ca^{2+} release via the Na^{+}/Ca^{2+} exchanger NCLX. This function was uncovered through studies with the fungal toxin phomoxanthone A (PXA), which induces NCLX-dependent Ca^{2+} release by directly targeting Mfn2. Mfn2-dependent Ca^{2+} release through NCLX is similarly triggered by ROS in respiring cells treated with oligomycin or mitoPQ. ROS enhances Ca^{2+} release by strengthening the interaction between Mfn2 and NCLX, an interaction that also requires the mitochondrial outer-membrane protein SLC25A46. Together, these proteins form a complex that coordinates mitochondrial fission and Ca^{2+} release to initiate mitophagy. Although the antioxidant N-acetylcysteine blocks ROS-induced mitochondrial fission, inhibition of Ca^{2+} release with the NCLX inhibitor CGP37157 does not, indicating that ROS-driven fission is independent of Ca^{2+} release. In contrast, Ca^{2+} release is required for efficient mitophagy, as NCLX inhibition arrests this process at a later stage. We further show that Ca^{2+} promotes mitophagy through NEDD4-1, which is a Ca^{2+}-responsive E3 ubiquitin ligase. Together, these findings connect mitochondrial ROS production to Ca^{2+} signaling, mitochondrial remodeling, and mitophagy, providing new insight into how mitochondrial dysfunction may contribute to neurodegenerative and metabolic disease.

Introduction

Fusion between mitochondrial outer membranes is mediated by the mitofusins Mfn1 and Mfn2 in mammals (Labbe *et al*, 2014). These proteins are dynamin-related GTPases with transmembrane segments anchored in the mitochondrial outer membrane (Santel & Fuller, 2001). Mutations in either mitofusin impair mitochondrial fusion and they are partially redundant with the ability to form heteromeric complexes (Chen *et al*, 2003), but they also have distinct functions. Mfn1 supports stress-induced mitochondrial hyperfusion (SIMH) (Tondera *et al*, 2009), while Mfn2 localizes to sites of mitochondrial fission at mitochondria-ER contact sites (MAMs) (Karbowski *et al*, 2002) and functions as a tether that promotes mitochondrial-ER association (de Brito & Scorrano, 2008). Through this role as a tether, Mfn2 influences several MAM-associated processes, including transfer of coenzyme Q (Mourier *et al*, 2015) and phosphatidylserine (Hernandez-Alvarez *et al*, 2019), as well as broader metabolic functions (Sebastian *et al*, 2012).

Mfn2-dependent ER-mitochondria contacts are also important for Ca^{2+} homeostasis (Wang *et al*, 2025b; Yang *et al*, 2023). Ca^{2+} released from the ER is taken up by the mitochondrial Ca^{2+} uniporter (MCU) in the inner membrane (De Stefani *et al*, 2015), while Ca^{2+} efflux occurs primarily through the Na^{+}/Ca^{2+} exchanger NCLX (Palty *et al*, 2010), which is regulated by PKA phosphorylation and membrane potential (Kostic *et al*, 2018; Kostic *et al*, 2015; Kostic & Sekler, 2019). Mitochondrial Ca^{2+} release can promote mitochondrial fragmentation via Ca^{2+}/calmodulin-dependent protein kinase I and II mediated phosphorylation of Drp1 (Han *et al*, 2008; Xu *et al*, 2016), and calcineurin mediated dephosphorylation (Cereghetti *et al*, 2008). AMP-activated protein kinase (AMPK), a central energy sensor, further links metabolism to mitochondrial dynamics. Under low-ATP conditions, AMPK promotes fission by phosphorylating the mitochondrial Drp1 receptor MFF (Toyama *et al*, 2016). AMPK also phosphorylates Mfn2 at serine 442 (Hu *et al*, 2021), a modification important for mitochondrial remodeling during metabolic stress. Mutations in MFN2 are the most common cause of axonal peripheral neuropathy, Charcot-Marie-Tooth type 2 (CMT2) (Verhoeven *et al*, 2006; Zuchner *et al*, 2004), but it remains unclear which Mfn2 functions are most relevant to the disease.

While studying previously described effects of the fungal metabolite phomoxanthone A (PXA) on mitochondrial Ca^{2+} release (Bohler *et al*, 2018), we discovered that these effects are suppressed by Mfn2 gene mutation. We then show that Mfn2 cooperates with NCLX to promote Ca^{2+} release, a process hinted at by previous findings showing that Mfn2 can drive reversal of NCLX in isolated mitochondria (Samanta *et al*, 2018). The outer-membrane protein SLC25A46 acts as an adaptor linking Mfn2 to NCLX; its deletion disrupts both mitochondrial Ca^{2+} release and Mfn2-NCLX association. ROS also induce Mfn2-dependent Ca^{2+} release via NCLX, prompting investigation of upstream regulatory steps and downstream physiological relevance of this pathway. We find that Oma1-mediated cleavage of Opa1 and PKA-mediated phosphorylation of NCLX both regulate ROS-induced Ca^{2+} release via NCLX. Downstream effects of ROS include AMPK-dependent fission and cytosolic Ca^{2+}-dependent activation of E3 ubiquitin ligases, which are essential for mitophagy. Overall, these findings reveal a mechanism relevant to neurodegenerative disease: mutations in these proteins cause defective mitophagy, impairing a vital quality-control process that removes damaged mitochondria.

Results

Mfn1 and Mfn2 have opposite effects on PXA-induced mitochondrial matrix contractions.

We previously described mitochondrial fragmentation and apoptosis caused by rapid mitochondrial Ca^{2+} release triggered by PXA (Bohler *et al.*, 2018). To avoid downstream effects of mitochondrial fragmentation and apoptosis (Wang *et al*, 2025a), we began using Drp1 KO cells in further investigations of the mechanisms underlying PXA-induced Ca^{2+} release. Knockouts were confirmed by Western blotting (Fig. S1A). Mutations in Drp1 prevent apoptosis and mitochondrial outer membrane fission, but PXA still induces excessive Ca^{2+} release, leading to mitochondrial matrix contraction. Drp1 KO cells treated with PXA exhibit a “beads on a string” or “pearling” phenotype (Stepp *et al*, 2026), due to the localized constrictions resulting from these matrix contractions (Fig. 1A,B).

Observing localized constrictions induced by PXA in Drp1 KO cells prompted us to investigate possible roles of other mitochondrial dynamics proteins in this process. The roles of Mfn1 and Mfn2 were assessed with Mfn1-Drp1 and Mfn2-Drp1 double-knockout (DKO) MEFs, as well as in Drp1-Mfn2 DKO HeLa cells, where Drp1 KO served to prevent apoptosis. Loss of each protein was confirmed by Western blotting (Fig. S1A). Strikingly, PXA elicited markedly different responses in Drp1-Mfn1 versus Drp1-Mfn2 DKO cells. Drp1-Mfn2 DKO MEFs and HeLa cells were completely resistant to PXA-induced matrix contraction, whereas Drp1-Mfn1 DKO cells exhibited enhanced matrix contraction compared with Drp1 knockout cells. In fact, this contraction was sufficient to drive mitochondrial fission even in the absence of Drp1 (Fig. 1A,B).

PXA-induced matrix retraction in Drp1 KO cells causes separation between outer-membrane and matrix fluorescence signals, visible in scatterplots (Fig. S1B). This separation enables quantification

using Manders' coefficients to assess the overlap between an outer-membrane marker (Tom20) and a matrix marker (Hsp60). Manders' coefficients showed a significant decrease in overlap in Drp1 KO cells treated with PXA, but not in Drp1-Mfn2 DKO cells. Conversely, the loss of overlap was more pronounced in Drp1–Mfn1 DKO cells (Fig. 1C,D). These findings suggest that Mfn2 inhibits PXA-induced contraction, while Mfn1 promotes it. This functional opposition aligns with previous siRNA studies in cardiomyocytes that demonstrated Mfn1 and Mfn2 differentially regulate mitochondrial Ca^{2+} uptake and release (Inagaki *et al*, 2023). Their opposing roles may arise from both their distinct functions and their ability to heterodimerize and counteract one another. In summary, Mfn2 is essential for PXA-induced mitochondrial matrix contraction and fission, whereas Mfn1 acts as an antagonist to this process.

Mfn2 controls mitochondrial Ca^{2+} release through NCLX when induced by PXA.

We focused on NCLX-mediated Ca^{2+} release because Mfn2 was previously shown to interact with and regulate NCLX (Samanta *et al.*, 2018). PXA-induced mitochondrial Ca^{2+} release was monitored in HeLa cells using a mitochondria-targeted fluorescent protein (R-Cepia3mt) and the vital dye Rhod-2 AM. HeLa cells were used throughout for Ca^{2+} release experiments because those cells yield good signal-to-noise ratios with the available probes. Single-cell Ca^{2+} traces were collected with the fluorescent protein using spinning-disk confocal microscopy (Fig. 2A,B), and population-level responses were measured with Rhod-2 AM using a plate reader (Fig. S2A,B). A CRISPR/Cas9-generated NCLX-KO HeLa line, validated by western blotting and comparison with NCLX-siRNA samples (Fig. S2A), was used as a control. Consistent with prior observations in WT cells (Bohler *et al.*, 2018), PXA caused rapid mitochondrial Ca^{2+} release in Drp1-KO cells (Fig. 2A,B, Fig. S2B-D). In contrast, this Ca^{2+} release was absent in Mfn2-Drp1 DKO cells, NCLX-KO cells, cells transfected with NCLX siRNA, and cells treated with the NCLX inhibitor CGP37157 (Fig. 2A,B). These findings demonstrate that PXA-induced mitochondrial Ca^{2+} release depends on both Mfn2 and NCLX.

We then assessed mitochondrial membrane potential, which was previously shown to decrease after PXA treatment, likely as a downstream effect of Ca^{2+} release. When NCLX exports Ca^{2+} in exchange for Na^+, the resulting mitochondrial Na^+ load is subsequently exchanged for protons via the mitochondrial Na^+/H^+ exchanger NHE1 (Fig. 2C) (Numata *et al*, 1998). This proton influx reduces the proton gradient and lowers the membrane potential. Our data show that PXA-induced membrane depolarization is prevented by Mfn2 loss and by CGP37157 (Fig. 2C-G). Depolarization is also slowed by the NHE1 inhibitor BIX, consistent with functional coupling between NCLX and NHE1. Therefore, the loss of mitochondrial membrane potential is an indirect result of NCLX activation by PXA. PXA-induced Ca^{2+} release does not occur in Mfn2-Drp1 DKO cells, indicating that it is specific to the role of Mfn2 in promoting NCLX activity. In contrast, treatment with CCCP causes Ca^{2+} release in all tested genotypes (Fig. S2E,F), demonstrating that this response does not require Mfn2 or NCLX. Ca^{2+} release induced by CCCP is likely mediated by reversal of MCU-mediated transport in mitochondria lacking membrane potential (Montero *et al*, 2001), unlike NCLX activity, which depends on membrane potential.

PXA interacts directly with Mfn2 in a complex with NCLX.

We used a cellular thermal shift assay (CETSA) to determine if PXA directly binds to Mfn2 or NCLX. In this assay, MEF extracts, solubilized with dodecyl maltoside, were incubated with PXA and subjected to a temperature gradient. After heat-induced denaturation, insoluble proteins were removed by centrifugation, and the remaining soluble proteins were analyzed by western blots. To evaluate shifts in denaturation temperature, we examined MEFs overexpressing Mfn2-FLAG and MEFs lacking Mfn1 or Mfn2. The functionality of Mfn2-FLAG was confirmed by its ability to rescue the mitochondrial morphology defect in Mfn2-KO cells (Fig. S3A). Since available NCLX antibodies recognize multiple nonspecific bands, we verified the identity of the NCLX band using KO controls (Fig. S3B, S3C). The CETSA results indicate that PXA shifts the denaturation temperatures of both Mfn1 and Mfn2, but not NCLX or SLC25A46, a mitochondrial outer membrane protein associated with Mitofusins and Opa1 (Steffen *et al*, 2017) (Fig. 3A,B). Vinculin, used as a control, remained unaffected. The thermal

stabilization by PXA was more pronounced in cells overexpressing Mfn2, supporting a direct interaction. Although PXA also influences Mfn1, suggesting it binds to additional proteins or conserved regions shared by Mfn1 and Mfn2, this does not change the essential role of Mfn2 in PXA-induced Ca^{2+} release. Several other targets of PXA were identified (Ali *et al*, 2022; Ceccacci *et al*, 2020), but the concentrations used in those studies were much higher than in our experiments, suggesting that they are not the primary cause of the morphological defects induced by PXA.

To determine whether Mfn2 directly interacts with NCLX, we conducted co-immunoprecipitation assays using epitope-tagged Mfn2-FLAG and chemical cross-linking. Mfn2-myc was confirmed to be functional by its ability to rescue the mitochondrial fusion defect in Mfn2 KO cells (Fig. S3A). Western blots showed increased co-immunoprecipitation of NCLX with Mfn2 after PXA treatment, along with a higher association of SLC25A46 (Fig. 3C-E). Conversely, co-immunoprecipitation of Calnexin decreased following PXA treatment, indicating that Mfn2 dissociates from the MAM under these conditions (Fig. 3F,G).

We further examined Mfn2-NCLX proximity using a Proximity Ligation Assay (PLA). Cells were transfected with Mfn2-myc and NCLX-HA, cultured under glycolytic conditions, and processed for PLA with myc and HA antibodies. Mitochondria were labeled using a chicken anti-Hsp60 antibody. PLA analysis showed an increased number of PLA puncta in glycolytic cells treated with PXA (Fig. 3H,I). PLA spots did not always coincide with Hsp60 staining because the mitochondrial matrix appears more condensed than the membranes where Mfn2 and NCLX are located. Co-staining with the outer membrane marker TOM20 confirmed that PLA signals originate from mitochondria (Fig. S3D). These findings demonstrate that Mfn2 and NCLX are in closer proximity after treatment with PXA or oligomycin. Overall, the results suggest that Mfn2 is essential for mitochondrial Ca^{2+} release via NCLX, and that this function is activated by PXA, which directly targets Mfn2.

Mfn2 controls ROS-induced mitochondrial Ca^{2+} release through NCLX.

Mitochondrial Ca^{2+} release is often monitored following extracellular histamine or ATP application, but these methods focus on the homeostatic functions of NCLX at the MAM. However, these approaches make it difficult to distinguish the tethering functions of Mfn2 at the MAM from a potential role as a regulator of NCLX without a detailed understanding of both functions. Instead, we assessed the physiological role of Mfn2-regulated Ca^{2+} release by NCLX under conditions that increase mitochondrial ROS. These conditions induce mitochondrial damage and, as a result, activate mitophagy to remove dysfunctional mitochondrial parts. Common methods for inducing mitophagy, such as CCCP or oligomycin/antimycin A treatments in glycolytic cells (Dong *et al*, 2023), were deemed uninformative because loss of mitochondrial membrane potential also prevents electrogenic Ca^{2+} release by NCLX. To maintain mitochondrial membrane potential, we induced ROS by treating respiring cells (grown with galactose) with oligomycin or mitoPQ. Oligomycin, an ATP synthase inhibitor, causes ATP depletion but also produces ROS in respiring cells through hyperpolarization of the mitochondrial inner membrane (Wilkins *et al*, 2022), while mitoPQ is a mitochondrial-targeted derivative of paraquat that uses electrons from the ETC to generate ROS (Antonucci *et al*, 2019).

We used N-acetyl cysteine (NAC) treatments to verify that effects on Ca^{2+} release and the Mfn2-NCLX complex are due to increased ROS levels. Cells were pre-incubated for 30 minutes with 5 mM NAC before inducing Ca^{2+} release with oligomycin and mitoPQ in WT HeLa cells grown under respiring conditions. As a control, we detected ROS with the ROS-sensitive dye mitoSOX. As expected, ROS levels increased with mitoPQ and oligomycin treatments and were reduced by pre-treatment with NAC (Fig. S4A). We found that oligomycin and mitoPQ treatments under respiring conditions (growth with galactose) induce mitochondrial Ca^{2+} release in HeLa cells, and this release can be blocked by quenching ROS with N-acetyl cysteine (NAC) (Fig. S4B, C), showing that ROS are needed for this response, even though, in the case of oligomycin, ROS are produced only as a secondary effect of ATP-synthesis inhibition. Since Ca^{2+} release by NCLX also depends on mitochondrial membrane potential, we tested whether ROS cause mitochondrial depolarization. It was previously reported that, as expected, oligomycin does not decrease mitochondrial membrane potential (Wilkins *et al.*, 2022), but we also

checked if mitoPQ affects membrane potential. Our results show that 50 and 100 μM mitoPQ do not impact mitochondrial membrane potential (Fig. S4D, E).

We used gene knockout to examine how Mfn2 and NCLX affect mitochondrial Ca^{2+} release triggered by oligomycin and mitoPQ. Knockouts of Mfn2 and NCLX were created in a Drp1 KO background to avoid complications from mitochondrial fragmentation during the assay. Our results show that Mfn2-Drp1 and NCLX-Drp1 DKO cells have impaired Ca^{2+} release, similar to what is seen with CGP37157 treatment (Fig. 4A-D). To confirm that these effects were due to specific gene knockdowns, we also tested siRNA effects. Successful knockdown of Mfn2 and NCLX in WT HeLa cells was confirmed by western blot (Fig. S4F). Similar to the effects of gene knockouts, Ca^{2+} release is also blocked by NCLX or MFN2 siRNA and by the NCLX inhibitor CGP37157 (Fig. S4G-J). The reduced mitochondrial Ca^{2+} observed suggests that Ca^{2+} is either released into the cytosol or transferred to other organelles, such as the ER or lysosomes. We tested this using a cytosolic Ca^{2+} sensor. Drp1 KO HeLa cells treated with oligomycin or mitoPQ showed a strong, sustained increase in cytosolic Ca^{2+} (Fig. 4E-H). This increase was prevented in Mfn2-Drp1 and NCLX-Drp1 DKO cells, as well as in Drp1 KO cells treated with CGP37157. We conclude that oligomycin and mitoPQ induce Ca^{2+} release into the cytosol of respiring HeLa cells, and this process requires both Mfn2 and NCLX.

To determine whether interactions between Mfn2 and NCLX are enhanced under ROS-inducing conditions, we performed PLA with Mfn2-myc and NCLX-HA and co-stained for mitochondria using chicken anti-Hsp60. We observed an increase in Mfn2/NCLX PLA puncta in cells treated with oligomycin or mitoPQ (Fig. 4I,J), indicating closer proximity between Mfn2 and NCLX under these conditions. We pretreated with NAC to test whether the association between Mfn2 and NCLX detected by PLA is promoted by ROS under these conditions. PLA for Mfn2 and NCLX, with or without pre-incubation with NAC, shows that NAC suppresses the association between Mfn2 and NCLX (Fig. S4K,L), which aligns with NAC's inhibitory effects on Ca^{2+} release. Having confirmed that Mfn2 associates more strongly with NCLX during stress and that Mfn2 is necessary for NCLX-dependent mitochondrial Ca^{2+} release, we then examined whether Mfn2's association with the MAM is similarly affected, using PLA for SERCA2 and transiently expressed Mfn2-myc in Drp1 KO MEFs. Treatment with oligomycin and mitoPQ, or in combination with the NCLX inhibitor CGP37157, each led to a significant decrease in Mfn2-SERCA2 PLA spots (Fig. 4K-N), suggesting reduced Mfn2 interaction with ER-mitochondria contact sites. These results indicate that oligomycin and mitoPQ increase Mfn2's association with NCLX, while they decrease Mfn2's association with SERCA2 at ER-mitochondrial contact sites.

SLC25A46 regulates Ca^{2+} release and the association between Mfn2 and NCLX.

To understand how Mfn2, which is anchored in the mitochondrial outer membrane with only a small part exposed to the intermembrane space, can regulate Ca^{2+} release by NCLX on the mitochondrial inner membrane, we examined several Mfn2-interacting proteins that have larger exposed regions in the intermembrane space as potential intermediaries between Mfn2 and NCLX. These proteins include Mtch1, Mtch2, MarchV, and SLC25A46. We focused on SLC25A46 because previous research showed that the mitochondrial fusion proteins (Mfn1, Mfn2, and Opa1) co-immunoprecipitate with this protein (Steffen *et al.*, 2017), and it plays a role in stress-induced mitochondrial dynamics (Schuettpelz *et al*, 2023).

Mitochondrial Ca^{2+} dynamics were observed in WT HeLa cells and cells transfected with SLC25A46 siRNA. Successful SLC25A46 knockdown was confirmed by Western blotting (Fig. S5A). Mitochondrial Ca^{2+} traces indicate that SLC25A46 knockdown decreases mitochondrial Ca^{2+} efflux triggered by oligomycin or mitoPQ under respiring conditions (Fig. 5A,B). To determine whether SLC25A46 is necessary for the interaction between Mfn2 and NCLX, we compared PLA signals for Mfn2-myc and NCLX-HA in Drp1 KO MEFs and SLC25A46-Drp1 double knockout cells, with or without oligomycin and mitoPQ treatments. The knockouts were verified by Western blot (Fig. S5B). The results show a nearly complete loss of Mfn2-NCLX spots when SLC25A46 is knocked out (Fig. 5C,D). These effects were confirmed with coIP of NCLX with Mfn2-FLAG in WT but not in SLC25A46 KO HeLa cells (Fig. 5E). SLC25A46 KO in HeLa cells and comparable levels of Mfn2-FLAG expression in stable cell

lines were validated with western blots (Fig. S5C,D). We conclude that SLC25A46 is essential for interactions between Mfn2 and NCLX, as well as for ROS-induced Ca^{2+} release.

Next, we examined interactions between SLC25A46 and NCLX and between Mfn2 and SLC25A46 to determine which pairs change under ROS-induced conditions. We observed more PLA spots with SLC25A46-myc and NCLX-HA in Drp1 KO cells treated with oligomycin or mitoPQ (Fig. 5F,G), along with increased coIP of NCLX-HA with SLC25A46-myc (Fig. S5E,F), but no increase in coIP of Mfn2 with SLC25A46 or vice versa of SLC25A46 with Mfn2 (Fig. S5G,H). These results indicate that the interactions between Mfn2 and SLC25A46 are stable, while those with NCLX depend on SLC25A46 and are induced by ROS.

Alternative pathways for control of mitochondrial Ca^{2+} release and fission.

Opa1 is a potential regulator of Mfn2-NCLX interactions, since Opa1 also interacts with SLC25A46 (Schuettpelz *et al.*, 2023; Steffen *et al.*, 2017). Opa1 is controlled by Oma1-mediated proteolytic cleavage (Ehses *et al*, 2009; Head *et al*, 2009), which is triggered by oligomycin in respiring cells (MacVicar & Lane, 2014), as also observed by us (Fig. S6A). To determine whether Oma1 influences Mfn2-NCLX interactions and Ca^{2+} release, we examined the effects in Oma1 KO HeLa cells (KO confirmed by Western blot, Fig. S6B) with or without oligomycin in respiring cells. We found that Oma1 KO prevented oligomycin-induced mitochondrial fragmentation in respiring cells, as shown by immunofluorescence images and aspect ratios (Fig. 6A, B). This lack of fission is like that observed in glycolytic Oma1 knockout cells treated with CCCP (Quiros *et al*, 2012). Moreover, PLA indicates that the oligomycin-induced increase in Mfn2-NCLX interactions is also blocked in Oma1 KO cells (Fig. 6C, D).

To confirm that Oma1 effects result from Opa1 loss due to cleavage, we tested the complete absence of Opa1 using Drp1-Opa1 DKO cells (DKO confirmed by Western blotting, Fig. S6C). These cells showed more PLA spots than WT cells, even without oligomycin treatment, and no further increase after oligomycin was applied (Fig. S6D, E). Mitochondrial Ca^{2+} release was blocked in Oma1 KO cells, like the effects seen with the NCLX inhibitor CGP37157 (Fig. 6E, F). We conclude that Oma1-mediated cleavage of Opa1 promotes oligomycin-induced mitochondrial fission and the interaction between Mfn2 and NCLX, which is essential for Ca^{2+} release. A model showing how Oma1 cleavage of Opa1 enables interactions between Mfn2, SLC25A46 and NCLX is depicted in Fig. S6F. Surprisingly, mitoPQ did not cause Opa1 cleavage in all cell types tested even though it still triggers Ca^{2+} release. These findings suggest that removing L-Opa1 during mitochondrial Ca^{2+} release is not always necessary. Oligomycin has been shown to induce Opa1 cleavage in respiring cells (MacVicar & Lane, 2014), and it may be more effective than mitopQ, because ATP deficiency by itself is a strong inducer of Opa1 cleavage (Baricault *et al*, 2007; Rainbolt *et al*, 2016). Further research is needed to understand how L-Opa1 influences the interactions between Mfn2 and NCLX.

It was previously shown that NCLX is also activated by PKA-mediated phosphorylation at Ser258 (Kostic *et al.*, 2015). We tested whether PKA is necessary for Ca2+ release induced by oligomycin and mitoPQ using the PKA inhibitor H89. The results demonstrate a block in Ca^{2+} release, indicating that PKA is essential for the ROS-induced activation of NCLX (Fig. 6G, H). To investigate this further, we expressed wild-type and phosphorylation-defective NCLX(S258A) in NCLX KO cells and treated them with oligomycin and mitoPQ. Expression levels of exogenously introduced NCLX were verified with Western blots (Fig. S6G). Cells expressing NCLX(S258A) showed impaired mitochondrial Ca^{2+} release compared to WT NCLX under ROS-inducing conditions (Fig. 6I, J). It was previously suggested that ROS can activate PKA via cysteine modification, thus bypassing cAMP-dependent activation (Ekhator *et al*, 2025; Zhang *et al*, 2016). This suggests that ROS and PKA act in a linear pathway to promote mitochondrial Ca^{2+} release, although independent mechanisms of control cannot yet be ruled out.

To determine whether mitochondrial ROS, Ca^{2+} release, or lack of ATP, as sensed by AMPK, contribute to the mitochondrial fission observed with oligomycin and mitoPQ, cells were pre-incubated with NAC (a ROS scavenger), CGP37157 (an NCLX inhibitor), or BAY-3827 (an AMPK inhibitor) before treatment with oligomycin or mitoPQ. Fission was assessed using immunofluorescence with Tom20, and

mitophagy was monitored with mitoQC. Oligomycin caused significant mitochondrial fragmentation, while mitoPQ resulted in a milder phenotype. Pre-incubation with CGP37157 partially reduced fragmentation in mitoPQ-treated cells, but the effect on oligomycin-treated cells was not statistically significant. In contrast, NAC and BAY-3827 both prevented mitochondrial fission induced by oligomycin or mitoPQ (Fig. S6H, I). Since AMPK is activated by ATP depletion, these results suggest that stress-induced fission in these cells is mainly driven by ATP depletion rather than increased cytosolic Ca^{2+}.

Mitochondrial Ca^{2+} efflux promotes mitophagy through the NEDD4-1 E3 ubiquitin ligase.

Instead of fission, Ca^{2+} release into the cytosol may influence other aspects of mitophagy. We tested this using the mitoQC reporter, a chimeric protein where GFP and mCherry are fused to the Fis1 tail anchor. Autophagolysosomes formed during mitophagy appear as red puncta because GFP is quenched in lysosomes. We found that oligomycin induces mitophagy in MEFs grown under respiring conditions, and this process is suppressed by NAC and CGP37157 (Fig. S7A,B). However, mitoPQ does not induce mitophagy in these cells, suggesting a more complex relationship between mitochondrial Ca^{2+} release and mitophagy. To explore whether cell-type-specific differences influence the ability of mitochondrial Ca^{2+} release to induce mitophagy, we examined its effects on mitophagy in SH-SY5Y cells. In these cells, both oligomycin and mitoPQ induce mitophagy, and this process is inhibited by NAC and CGP37157 (Fig. 7A-D). These findings suggest that SH-SY5Y cells, unlike MEFs, contain a Ca^{2+}-sensitive factor that enables mitoPQ-induced mitophagy.

To identify which mitophagy factors might detect mitochondrial Ca^{2+} release, we performed a targeted siRNA screen focusing on E3 ubiquitin ligases that could respond to cytosolic Ca^{2+}. These include NEDD4-1 (Plant *et al*, 2000), NEDD4-L (Han *et al*, 2024), and SMURF1 (Lu *et al*, 2011), all of which have C2 domains, as well as TRIM5α (Saha *et al*, 2024)\ and UBE3 (Braganza *et al*, 2017). We found that NEDD4-1 siRNA reduces mitophagy induced by oligomycin and mitoPQ in SH-SY5Y cells, while siRNA against the other ligases has little or no effect (Fig. S7C-F). Knockdown was verified with Western blots (Fig. S7G). To verify that NEDD4-1 promotes Ca^{2+}-induced mitophagy, we transfected HeLa cells with constructs expressing NEDD4-1 and Parkin (HeLa cells lack Parkin), or Parkin alone. Our results show that the combination of the two proteins, but not Parkin alone, significantly increases the number of autophagolysosomes formed in response to mitoPQ and oligomycin (Fig. 7E-F). Expression of NEDD4-1 was verified with Western blots (Fig. S7H). Parkin is likely required to initiate mitophagy when damaged mitochondrial fragments are generated, because these fragments lose membrane potential (Twig *et al*, 2008; Youle & van der Bliek, 2012). However, the role of NEDD4-1 in this process is novel. We conclude that NEDD4-1 promotes Ca^{2+}-induced mitophagy in respiring cells. This effect is therefore dependent on NEDD4-1 expression levels, whereas in glycolytic HeLa cells, transfection with Parkin alone is sufficient to promote CCCP-induced mitophagy (Narendra *et al*, 2008).

Together, these results support a pathway in which ROS and PKA facilitate mitochondrial Ca^{2+} release by promoting interactions between NCLX, Mfn2, and SLC25A46 (Fig. 7G). Oma1-mediated cleavage of Opa1 strengthens these interactions while downstream effects of Ca^{2+} release on mitophagy through NEDD4-1 complement the effects of AMPK on mitochondrial fission and ULK1 activation during mitophagy (Iorio *et al*, 2021).

Discussion

Mitochondria-derived ROS is widely implicated in redox signaling and stress responses. However, the molecular mechanism by which ROS generated within mitochondria are translated into cytosolic signaling events that report mitochondrial dysfunction remains poorly understood. Here, we demonstrate that ROS induces NCLX-mediated mitochondrial Ca^{2+} release in an Mfn2-dependent manner, and this in turn promotes mitophagy. We identify three key elements: (1) the upstream ROS-dependent signals that trigger Ca^{2+} release, (2) a protein complex spanning the mitochondrial inner and outer membranes that enables this release, and (3) downstream Ca^{2+}-dependent steps required for ROS-induced mitophagy in respiring cells. The newly uncovered role of Mfn2 in regulating mitochondrial Ca^{2+} release represents a

novel function, adding to its well-known roles as a mitochondrial fusion protein (Chen *et al.*, 2003) and as a tether linking mitochondria and the ER (de Brito & Scorrano, 2008).

We find that ROS produced by respiring cells treated with oligomycin or mitoPQ acts as a signal that induces mitochondrial Ca^{2+} release. As part of this process, ROS promotes the association between Mfn2 and NCLX. This increased association is triggered by OMA1-dependent cleavage of OPA1. Our data suggest that Opa1 cleavage clears the way for interactions between Mfn2 and NCLX, because these interactions constitutively increase when Opa1 is fully removed in KO cells. ROS-induced Ca^{2+} release is further regulated by PKA-dependent phosphorylation of NCLX, which may act upstream or alongside ROS-driven signals that stimulate NCLX activity, adding to previous studies of PKA-regulated NCLX activity (Kostic *et al.*, 2015).

The ROS-driven pathway for Ca^{2+} release outlined here begins within mitochondria and fundamentally differs from homeostatic fission driven by external Ca^{2+} signals, such as ER Ca^{2+} release or ionomycin-induced Ca^{2+} influx. These external pathways activate INF2-dependent actin assembly at mitochondria-ER contact sites (MAMs) (Korobova *et al*, 2014; Korobova *et al*, 2013) and rely on mitochondrial Ca^{2+} uptake rather than OMA1 activity (Chakrabarti *et al*, 2018; Fung *et al*, 2023). However, it is still possible that mitochondrial Ca^{2+} release during mitophagy is also triggered by external signals, such as PINK1- or PKA-dependent phosphorylation of Mfn2, because these are also accompanied by the dissociation from the ER (Chen & Dorn, 2013; Dasgupta *et al*, 2021; Zhou *et al*, 2010). It remains to be seen whether the ROS-driven pathway described here occurs at mitochondrial tips (Kleele *et al*, 2021) and involves lysosome-driven mechanisms of fission (Kleele *et al.*, 2021; Peng *et al*, 2020; Wong *et al*, 2019; Wong *et al*, 2018). Nonetheless, this pathway provides new opportunities for studying how mitochondria identify, segregate, and eliminate damaged regions through mitophagy (Twig *et al.*, 2008; Youle & van der Bliek, 2012).

The Mfn2/NCLX protein complex that mediates ROS-induced Ca^{2+} release includes SLC25A46 on the outer membrane. SLC25A46 interacts with both Mfn1 and Mfn2 on the outer membrane(Steffen *et al.*, 2017), but there are fundamental differences between the roles of Mfn1 and Mfn2: Mfn1 cooperates with L-OPA1 to promote stress-induced mitochondrial hyperfusion (Tondera *et al.*, 2009), while Mfn2 acts as an ER–mitochondria tether at the MAM (de Brito & Scorrano, 2008) and, as shown here, helps facilitate mitochondrial Ca^{2+} release. Whether these functional differences arise from distinct binding modes between Mfn1 or Mfn2 and SLC25A46, or involve other factors, remains to be determined. TMEM65, another inner membrane protein, has been reported to associate with NCLX and regulate its activity (Garbincius *et al*, 2025). Although still debated (Garbincius & Elrod, 2025), it has even been suggested to mediate Na^{+}/Ca^{2+} exchange independently of NCLX (Vetralla *et al*, 2025; Zhang *et al*, 2025). However, our data show that NCLX is essential for ROS-induced mitochondrial Ca^{2+} release, since no Ca^{2+} release is observed in NCLX-deficient cells, in line with the proposal that TMEM65 acts through NCLX interactions.

Downstream effects of Ca^{2+} release by the Mfn2/NCLX complex were not as expected directly involved in fission. Cytosolic Ca^{2+} was previously shown to promote mitochondrial fission through Drp1 activation, either via CaMK-I/II–dependent phosphorylation at residue 616 (Han *et al.*, 2008; Xu *et al.*, 2016) or through calcineurin-dependent dephosphorylation at residue 637 (Cereghetti *et al.*, 2008; Cribbs & Strack, 2007), but our data suggest that mitochondrial ROS-induced fission is largely independent of mitochondrial Ca^{2+} efflux, as inhibition of NCLX had only minor effects on fission. Instead, the stronger effects of inhibiting AMPK suggest that stress-induced fission is primarily mediated by AMPK-dependent phosphorylation of MFF (Toyama *et al.*, 2016), likely driven by ATP depletion resulting from oxidative stress.

Instead of fission, our data shows that ROS-induced Ca^{2+} release functions at a different stage of mitophagy. Rather than directly inducing fission, ROS-induced Ca^{2+} release acts through the Ca^{2+}-regulated E3 ubiquitin ligase NEDD4-1, which we show is required for the progression of ROS-induced mitophagy. NEDD4-1 contains a Ca^{2+}-binding C2 domain that associates with PI(3)P on autophagic membranes, as well as an LC3-interacting region (LIR) that can bind to LC3 on phagophore membranes (Sun *et al*, 2017). NEDD4-1 polyubiquitinates SQSTM1/p62 (Lin *et al*, 2017), enhancing its receptor activity and stabilizing protein complexes with autophagic cargo (Kumar *et al*, 2022; Peng *et al*, 2017;

Xiao *et al*, 2025). NEDD4-1 may work in concert with other E3 ubiquitin ligases that initiate mitophagy by ubiquitinating mitochondrial outer membrane proteins (Wang *et al*, 2026). Support for a pro-autophagic role of Ca^{2+} release comes from an OPA1 heterozygous mouse model showing chronic mitochondrial Ca^{2+} release, excessive mitophagy, and cell death (Zaninello *et al*, 2022), likely due to impaired NCLX retention in cristae and increased interactions between NCLX and Mfn2. NCLX has been implicated in actin polymerization via ARP2/3 (Chakrabarti *et al*, 2022), likely via Ca^{2+}/calmodulin (Sadhu *et al*, 2023). This type of actin polymerization interferes with Parkin-dependent mitophagy triggered by loss of membrane potential using CCCP (Fung *et al*, 2025). Our ROS treatments, however, maintain mitochondrial potential, suggesting a mechanism distinct from depolarization-induced mitophagy.

Mfn2-dependent regulation of mitochondrial Ca^{2+} release may play a crucial role in diseases caused by MFN2 mutations, such as Charcot-Marie-Tooth disease type 2A and cardiomyopathy, where mitophagy defects have been observed (Franco *et al*, 2023). Interestingly, defects in PINK1 lead to mitochondrial Ca^{2+} overload and necrosis (Gandhi *et al*, 2009), possibly because Mfn2 remains attached to the MAM, while PKA-dependent NCLX activation reduces Ca^{2+} overload in PINK1-deficient cells (Kostic *et al.*, 2015). This suggests a common mechanism linking Mfn2 regulation, Ca^{2+} balance, and disease development. These defects may operate simultaneously or worsen pre-existing disruptions in mitochondrial fusion, transport (Stuppia, 2015 #4401; Zhou, 2019 #5159), and ER-mitochondria tethering (Bernard-Marissal, 2019 #4946) caused by mutations in Mfn2.

In summary, our results support a model where ROS triggers mitochondrial Ca^{2+} release through coordinated regulation of Mfn2, SLC25A46 and NCLX. The resulting Ca^{2+} signal promotes mitophagy rather than fission, establishing a distinct, mitochondria-originating stress response pathway that integrates redox signaling, mitochondrial dynamics, and quality control.

Materials and methods

Antibodies and chemicals: Rabbit polyclonal anti-Mfn1, NCLX, SLC25A46, and Tomm20 antibodies were from ProteinTech. Rabbit polyclonal anti-Mfn2 and Oma1 antibodies were from Cell Signaling. Rabbit polyclonal anti-Vinculin and Myc antibodies were from Sigma. Mouse monoclonal anti-Tubulin and Actin antibodies were from Sigma. Mouse monoclonal anti-CNX, Opa1 and Drp1 antibodies were from BD Pharmingen. Mouse monoclonal anti-Hsp60 antibodies were from Abcam. Mouse monoclonal anti-FLAG antibodies were from Proteintech. Mouse monoclonal anti-HA antibodies were from Millipore. Chicken polyclonal ant-Hsp60 antibodies were from EnCor. Oligomycin, Antimycin, CGP37157, CCCP, TMRM, DSP, SPDP and Dodecyl-maltoside were from Sigma. PXA was from Adipogene. Rhod-2AM was from Biotium. FLAG Magnetic Beads were from Pierce. BIX was from Tocris.

DNA and RNA: The Mfn2-16xmyc, pCMV R-Cepia3mt and px459 plasmids were from Addgene (#23213, #140464 and #62988, respectively). The pPB EF1A>hNCLX-3xHA and pPB EF1A>hMfn2-3xFlag and pBase plasmids were from Vectorbuilder. The pCDNA3 hMfn2-FLAG plasmid was a kind gift from Gerald Dorn (Washington University). Target sites for gene deletions were identified using the Boutros Lab Website (http://www.e-crisp.org/E-CRISP/designcrispr.html) or as recommended by the Vectorbuilder website. The gRNAs were cloned in the px459 plasmid or in a custom vector from Vectorbuilder. The gRNAs used in this study are listed in Table 1. NCLX expression was knocked down in MEFs with shRNA as described (Palty *et al.*, 2010) and in HeLa cells with mixture of 2 predesigned Dicer-Substrate siRNAs from IDT (cat nr. hs.Ri.SLC8B1.13.2 and hs.Ri.SLC8B1.13.3. Site-directed mutagenesis used the DpnI-method for double-strand plasmids(Braman *et al*, 1996; Kolitsida *et al*, 2019).

Cell culture, transfections and gene knockouts. HeLa cells were from James Wohlschlegel (Dept. of Biological Chemistry, UCLA) and MEFs were from David Chan (Dept of Biology, CalTech). Cells were grown in glycolytic medium (DMEM with 10% FBS with 1% Pen/Strep and 4.5 g/l glucose) or respiring medium (DMEM without glucose and supplemented with 4.5g/L galactose, 10% FBS, 1% PS, 5mM sodium pyruvate and 2mM L-glutamine) as indicated. All cell lines were periodically checked for Mycoplasm. Transient transfections were done with jetPRIME following manufacturer's instructions (Polyplus). For siRNA, cells were grown in 6cm dishes, transfected with 50nM oligonucleotides using

RNAimax (Invitrogen) and analyzed 72h later. For gene knockouts, 1.2µg/well was transfected into 6 well plates cells, followed by selection at increasing concentrations or puromycin from 1µg to 5 µg/ml for 1-2 days. Surviving colonies were isolated and analyzed with Western blots. A stable cell line that expresses human Mfn2 with 3XFLAG under the EF1alpha promoter was generated with a PiggyBac construct from Vectorbuilder. This construct was transfected into Drp1/Mfn2 DKO MEFs along with the PBase vector from Vectorbuilder at equal concentrations (2µg/per well in a 6 well plate). At 24h post transfection, cells were subjected to puromycin selection at increasing concentrations from 1µg to 5 µg/ml for 1-2 days.

After selection, surviving colonies were isolated with cloning rings, expanded and analyzed for Mfn2 expression levels by Western blotting.

For lentiviral transduction, cells were seeded in 6-well plates at a density of 1.5–2 × 10^5 cells per well to achieve 50–70% confluency at the time of infection. On the day of transduction, the culture medium was replaced with fresh complete medium containing polybrene (5 µg/mL final concentration) to enhance viral entry. A concentrated lentiviral stock for mitoQC (Welgen Inc) was diluted 1:1000 in complete medium and added dropwise to the cells. Cells were incubated with the virus-containing medium for 48 h at 37 °C. After this period, the viral supernatant was removed and fresh complete medium without polybrene was added. Transduction efficiency was assessed 72 h post-infection by fluorescence microscopy for GFP/RFP expression.

Immunoblotting and immunofluorescence: Total cell lysates for Western blotting were prepared in RIPA buffer. Samples were subjected to SDS-PAGE, transferred to PVDF membranes, blocked with 5% non-fat milk, and incubated overnight at 4 °C with primary antibodies. Membranes were then washed with TBS- T and incubated with secondary antibodies. Chemiluminescent bands were detected with a BioRad scanner. For immunofluorescence images, cells were grown on 12mm coverslips, fixed for 15min with 4% paraformaldehyde in PBS, and permeabilized for 15min with 0.25% Triton X-100 in PBS, blocked for 1h with BSA in PBS-T and incubated with primary antibodies. Secondary antibodies were Alexa Fluor 488-, 594- or 647-conjugated goat anti-mouse or rabbit IgG (Invitrogen).

Proximity ligation assays were conducted with Duolink as recommended by the manufacturer (Sigma-Aldrich). Cells were seeded on coverslips and at 60% confluency they were transfected with Mfn2-myc and NCLX-HA overnight. The cells were then treated for 5-10 min with 10µM PXA or for 30min 10µM oligomycin or DMSO as indicated, after which they were processed for PLA as described (Alam, 2018), but with the following modification: After the fixation and washing, cells were permeabilized with 0.3% Triton-X100 for 10 minutes at room temperature and then washed twice for 5 min with PBS. Along with the primary antibodies for PLA, we also added chicken anti-HSP60 antibody (EnCor Biotechnology Inc) or TOM20 (Proteinteck) and anti-chicken or anti rabbit Alexa Fluor 488 as secondary antibody, along with the primary and secondary antibodies for PLA.

Microscopy was performed with a Marianas spinning disc confocal from Intelligent Imaging, which uses an Axiovert microscope (Carl Zeiss Microscopy) with 40x/1.4 and 100x/1.4 oil objectives, a CSU22 spinning disk (Yokogawa), an Evolve 512 EMCCD camera (Photometrics), and a temperature unit (Okolab). For live cell imaging, cells were grown in glass bottom dishes (MatTek) and imaged in situ at 37°C. Fiji software was used to determine Manders' coefficients and generate scatter plots. Aspect ratios of mitochondria were determined with Tomm20 fluorescence images. First, cells in the images were demarcated using FIJI ImageJ (https://fiji.sc/). Mitochondria were then demarcated using CellProfiler (https://cellprofiler.org/), and background noise was suppressed with a median filter. Mitochondria were segmented with a global, three-class, Otsu-thresholding method, minimizing the weighted-variance to shape. The aspect ratio of each object was then determined as the quotient of Major Axis Length over Minor Axis Length. Data represent the average aspect ratio for 25 cells in 3 independent experiments using WT and Oma1 KO HeLa cells.

Mitochondrial Ca2+ levels were determined in HeLa cells with transiently transfected pCMV R-Cepia3mt (Addgene #140464). Transfected cells were first perfused for 30 min with HBSS to record a baseline signal. Where indicated 10 µM CGP37157 or 10 µM BIX was included with the perfusion. Mitochondrial Ca^{2+} release was then triggered by adding 10 µM PXA or 10 µM Oligomycin. Using 3I software,

fluorescence intensities of individual cells was determined once per second over a period of 10 min after the addition of PXA or Oligomycin. Mitochondrial calcium levels in MEFs were measured using a Tecan Spark 10M multimode plate reader equipped with an injector, as previously described (Martinez *et al*, 2017). In brief, MEF DRP1 KO or double MFN2/DRPI KO cells were plated on Corning 96 Flat black, clear bottom wells and loaded with 1 μM Rhod2-AM for 30 min at 37 °C using a modified Krebs–Ringer's solution containing (126 mM NaCl, 5.4 mM KCl, 0.8 mM $MgCl_2$, 20 mM HEPES, 1.8 mM $CaCl_2$, 15 mM glucose, with pH adjusted to 7.4 with NaOH and supplemented with 0.1% BSA). After dye loading, cells were washed three times with fresh dye-free Krebs–Ringer's solution, followed by additional incubation of 30 min to allow for the de-esterification of the residual dye. Kinetic live-cell fluorescent imaging was performed to monitor Ca^{2+} transients. Rhod2-AM was excited at 552 nm wavelength light and imaged with a 570 nm. After establishing a baseline, cells were triggered with PXA at a final concentration of 10 μM. Kinetic measurements were taken at ~ 5 s intervals. Traces of Ca^{2+} responses were analyzed and plotted using KaleidaGraph. The rate of ion transport was calculated from each graph (summarizing an individual experiment) by a linear fit of the change in the fluorescence over time ($\Delta F/dt$), as previously described (Assali *et al*, 2020; Taha *et al*, 2024).

Cytosolic Ca^{2+} levels in HeLa cells were determined after loading with Calbyte-520aAM for 30min at RT using a Krebs–Ringer's solution containing (126 mM NaCl, 5.4 mM KCl, 0.8 mM $MgCl_2$, 20 mM HEPES, 1.8 mM $CaCl_2$, adjusted to pH 7.3 with NaOH). After dye loading cells were washed three times with PBS, followed by additional incubation of 30 min to allow for the de-esterification of the residual dye. Calbryte 520-AM was excited at 488 nm wavelength light and imaged with a 520 nm. These transfected cells were first perfused for 30 min with Krebs-Ringer's solution included the treatment 10 μM CGP37157. Cytosolic Ca^{2+} release was then triggered by adding 10 μM Oligomycin or 50μM mitoPQ. Using 3I software, fluorescence intensities of individual cells was determined once per second over a period of 10 min after the addition of oligomycin or mitoPQ.

Mitochondrial membrane potential was detected with TMRM (Thermo-Fisher Scientific). Cells plated in 35 mm glass bottom dishes (MatTek) were rinsed with 10 mM HEPES buffered HBSS, pH 7.3 with 15 mM glucose and subsequently incubated with 25 nM TMRM for 30 min at 37°C, followed by 3 washes with PBS and destaining for 30 min at 37°C in 1.8mM $CaCl_2$, 120mM NaCl, 5.4mM KCl, 0.8mM $MgCl_2$, 20mM HEPES, 15mM glucose, adjusted to pH 7.3 with NaOH. Fluorescence images were acquired for a field of cells with 10x objective. Where indicated, cells were treated for 30 min at 37°C with 10 μM CGP37157 or 100 nM BIX before adding 10 μM PXA. As a reference for uncoupling, cells were treated with 10 μM CCCP.

Cellular Thermal Shift Assay (CETSA): MEFs cultured to 1.0×10^7 cells in a 15 cm dish were washed with PBS and harvested in 2 ml lysis buffer (1.8mM CaCl2, 120mM NaCl, 5.4mM KCl, 0.8mM MgCl2, 20mM HEPES, 15mM glucose, 0.5% Dodecyl-Maltoside, adjusted to pH 7.3 with NaOH). Equal volumes of cell lysates were transferred to 1.5 ml Eppendorf tubes for incubation with 1 μM PXA or DMSO for 4 min at RT. After this incubation, 100 μl aliquots of cell lysates were transferred to PCR tubes and heated on a gradient PCR machine for 3 min at different temperatures as indicated and then cooled to 25°C for 2 min, followed by centrifugation for 30 min at 20.000g in 4 °C. Supernatants were then transferred to new tubes with sample buffer. For each temperature, 10 μl (approximately 30 μg protein) was analyzed by SDS-PAGE and western blotting. Band intensities were quantified with densitometry and ImageJ.

Co-immunoprecipitation MEFs stably expressing Mfn2-FLAG were treated for 5 minutes at 37 °C with DMSO, 10μM PXA, 10μM CCCP, or 10μM CGP37157 as indicated. These cells were then washed with ice cold PBS with 0.9 mM $CaCl_2$ and 0.5 mM $MgCl_2$ and crosslinked for 2h on ice with 1 mM DSP or 1 mM BMH. The crosslinkers were then quenched by incubating for 15 minutes on ice with 20 mM Tris-Cl (pH7.4) followed by a wash with ice cold PBS with 0.9 mM $CaCl_2$ and 0.5 mM $MgCl_2$ and resuspending in RIPA buffer. Co-immunoprecipitations were conducted with 1 mg protein (determined with BCA assay). 50 μl of magnetic FLAG beads (Pierce/Sigma) per sample were washed twice with 1X TBST and then incubated with protein samples for 45min at 4 °C on a rotor. Beads were then collected using a magnetic stand and the supernatant was discarded. The beads were washed twice with 1X TBST and then once

with ddH2O. Finally, the beads were resuspended in 50 µl of 2X sample buffer, heated for 5 min at 95 °C, and analyzed by western blot.

Statistics & reproducibility: All statistical analyses were performed on Graphpad Prism Version 8.4.1. All column graphs were generated on Graphpad Prism Version 8.4.1. Data points from all biological replicates were tested for multiple comparison using Turkey test and ANOVA test. The bars indicate standard deviations. Each data point on a column graph represents one biological replicate. All quantitative analysis was performed on at least three biological replicates per condition. Data are represented as mean, and error bars indicate the standard deviation of the mean.

Acknowledgements

CMK was supported by NIH grants R01GM61721, R01GM073981 and R01DK101780. AMvdB was supported by NIH grants U01GM109764 and R01NS120690.

References

Alam MS (2018) Proximity Ligation Assay (PLA). *Curr Protoc Immunol* 123: e58

Ali R, Parelkar SS, Thompson PR, Mitroka-Batsford S, Yerramilli S, Scarlata SF, Mistretta KS, Coburn JM, Mattson AE (2022) Phomoxanthone A Targets ATP Synthase. *Chemistry* 28: e202202397

Antonucci S, Mulvey JF, Burger N, Di Sante M, Hall AR, Hinchy EC, Caldwell ST, Gruszczyk AV, Deshwal S, Hartley RC *et al* (2019) Selective mitochondrial superoxide generation in vivo is cardioprotective through hormesis. *Free Radic Biol Med* 134: 678-687

Assali EA, Jones AE, Veliova M, Acin-Perez R, Taha M, Miller N, Shum M, Oliveira MF, Las G, Liesa M *et al* (2020) NCLX prevents cell death during adrenergic activation of the brown adipose tissue. *Nat Commun* 11: 3347

Baricault L, Segui B, Guegand L, Olichon A, Valette A, Larminat F, Lenaers G (2007) OPA1 cleavage depends on decreased mitochondrial ATP level and bivalent metals. *Exp Cell Res* 313: 3800-3808

Bohler P, Stuhldreier F, Anand R, Kondadi AK, Schlutermann D, Berleth N, Deitersen J, Wallot-Hieke N, Wu W, Frank M *et al* (2018) The mycotoxin phomoxanthone A disturbs the form and function of the inner mitochondrial membrane. *Cell Death Dis* 9: 286

Braganza A, Li J, Zeng X, Yates NA, Dey NB, Andrews J, Clark J, Zamani L, Wang XH, St Croix C *et al* (2017) UBE3B Is a Calmodulin-regulated, Mitochondrion-associated E3 Ubiquitin Ligase. *J Biol Chem* 292: 2470-2484

Braman J, Papworth C, Greener A (1996) Site-directed mutagenesis using double-stranded plasmid DNA templates. *Methods Mol Biol* 57: 31-44

Ceccacci S, Deitersen J, Mozzicafreddo M, Morretta E, Proksch P, Wesselborg S, Stork B, Monti MC (2020) Carbamoyl-Phosphate Synthase 1 as a Novel Target of Phomoxanthone A, a Bioactive Fungal Metabolite. *Biomolecules* 10

Cereghetti GM, Stangherlin A, Martins de Brito O, Chang CR, Blackstone C, Bernardi P, Scorrano L (2008) Dephosphorylation by calcineurin regulates translocation of Drp1 to mitochondria. *Proceedings of the National Academy of Sciences of the United States of America* 105: 15803-15808

Chakrabarti R, Fung TS, Kang T, Elonkirjo PW, Suomalainen A, Usherwood EJ, Higgs HN (2022) Mitochondrial dysfunction triggers actin polymerization necessary for rapid glycolytic activation. *J Cell Biol* 221

Chakrabarti R, Ji WK, Stan RV, de Juan Sanz J, Ryan TA, Higgs HN (2018) INF2-mediated actin polymerization at the ER stimulates mitochondrial calcium uptake, inner membrane constriction, and division. *J Cell Biol* 217: 251-268

Chen H, Detmer SA, Ewald AJ, Griffin EE, Fraser SE, Chan DC (2003) Mitofusins Mfn1 and Mfn2 coordinately regulate mitochondrial fusion and are essential for embryonic development. *J Cell Biol* 160: 189-200

Chen Y, Dorn GW, 2nd (2013) PINK1-phosphorylated mitofusin 2 is a Parkin receptor for culling damaged mitochondria. *Science* 340: 471-475

Cribbs JT, Strack S (2007) Reversible phosphorylation of Drp1 by cyclic AMP-dependent protein kinase and calcineurin regulates mitochondrial fission and cell death. *EMBO Rep* 8: 939-944

Dasgupta A, Chen KH, Lima PDA, Mewburn J, Wu D, Al-Qazazi R, Jones O, Tian L, Potus F, Bonnet S *et al* (2021) PINK1-induced phosphorylation of mitofusin 2 at serine 442 causes its proteasomal degradation and promotes cell proliferation in lung cancer and pulmonary arterial hypertension. *FASEB J* 35: e21771

de Brito OM, Scorrano L (2008) Mitofusin 2 tethers endoplasmic reticulum to mitochondria. *Nature* 456: 605-610

De Stefani D, Patron M, Rizzuto R (2015) Structure and function of the mitochondrial calcium uniporter complex. *Biochim Biophys Acta* 1853: 2006-2011

Dong Y, Zhuang XX, Wang YT, Tan J, Feng D, Li M, Zhong Q, Song Z, Shen HM, Fang EF *et al* (2023) Chemical mitophagy modulators: Drug development strategies and novel regulatory mechanisms. *Pharmacol Res* 194: 106835

Ehses S, Raschke I, Mancuso G, Bernacchia A, Geimer S, Tondera D, Martinou JC, Westermann B, Rugarli EI, Langer T (2009) Regulation of OPA1 processing and mitochondrial fusion by m-AAA protease isoenzymes and OMA1. *J Cell Biol* 187: 1023-1036

Ekhator ES, Fazzari M, Newman RH (2025) Redox Regulation of cAMP-Dependent Protein Kinase and Its Role in Health and Disease. *Life (Basel)* 15

Franco A, Li J, Kelly DP, Hershberger RE, Marian AJ, Lewis RM, Song M, Dang X, Schmidt AD, Mathyer ME *et al* (2023) A human mitofusin 2 mutation can cause mitophagic cardiomyopathy. *Elife* 12

Fung TS, Chakrabarti R, Higgs HN (2023) The multiple links between actin and mitochondria. *Nat Rev Mol Cell Biol* 24: 651-667

Fung TS, Ghosh A, Zavala MR, Nichtova Z, Shukal D, Tigano M, Csordas G, Higgs HN, Chakrabarti R (2025) Peri-mitochondrial actin filaments inhibit Parkin assembly by disrupting ER-mitochondria contacts. *EMBO Rep* 26: 4977-5008

Gandhi S, Wood-Kaczmar A, Yao Z, Plun-Favreau H, Deas E, Klupsch K, Downward J, Latchman DS, Tabrizi SJ, Wood NW *et al* (2009) PINK1-associated Parkinson's disease is caused by neuronal vulnerability to calcium-induced cell death. *Mol Cell* 33: 627-638

Garbincius JF, Elrod JW (2025) Mitochondrial sodium-calcium exchange-Can TMEM65 do it alone? *Cell Metab* 37: 1927-1928

Garbincius JF, Salik O, Cohen HM, Choya-Foces C, Mangold AS, Makhoul AD, Schmidt AE, Khalil DY, Doolittle JJ, Wilkinson AS *et al* (2025) TMEM65 regulates and is required for NCLX-dependent mitochondrial calcium efflux. *Nat Metab* 7: 714-729

Han F, Wu S, Dong Y, Liu Y, Sun B, Chen L (2024) Aberrant expression of NEDD4L disrupts mitochondrial homeostasis by downregulating CaMKKbeta in diabetic kidney disease. *J Transl Med* 22: 465

Han XJ, Lu YF, Li SA, Kaitsuka T, Sato Y, Tomizawa K, Nairn AC, Takei K, Matsui H, Matsushita M (2008) CaM kinase I alpha-induced phosphorylation of Drp1 regulates mitochondrial morphology. *J Cell Biol* 182: 573-585

Head B, Griparic L, Amiri M, Gandre-Babbe S, van der Bliek AM (2009) Inducible proteolytic inactivation of OPA1 mediated by the OMA1 protease in mammalian cells. *J Cell Biol* 187: 959-966

Hernandez-Alvarez MI, Sebastian D, Vives S, Ivanova S, Bartoccioni P, Kakimoto P, Plana N, Veiga SR, Hernandez V, Vasconcelos N *et al* (2019) Deficient Endoplasmic Reticulum-Mitochondrial Phosphatidylserine Transfer Causes Liver Disease. *Cell* 177: 881-895 e817

Hu Y, Chen H, Zhang L, Lin X, Li X, Zhuang H, Fan H, Meng T, He Z, Huang H *et al* (2021) The AMPK-MFN2 axis regulates MAM dynamics and autophagy induced by energy stresses. *Autophagy* 17: 1142-1156

Inagaki S, Suzuki Y, Kawasaki K, Kondo R, Imaizumi Y, Yamamura H (2023) Mitofusin 1 and 2 differentially regulate mitochondrial function underlying Ca(2+) signaling and proliferation in rat aortic smooth muscle cells. *Biochem Biophys Res Commun* 645: 137-146

Iorio R, Celenza G, Petricca S (2021) Mitophagy: Molecular Mechanisms, New Concepts on Parkin Activation and the Emerging Role of AMPK/ULK1 Axis. *Cells* 11

Karbowski M, Lee YJ, Gaume B, Jeong SY, Frank S, Nechushtan A, Santel A, Fuller M, Smith CL, Youle RJ (2002) Spatial and temporal association of Bax with mitochondrial fission sites, Drp1, and Mfn2 during apoptosis. *J Cell Biol* 159: 931-938

Kleele T, Rey T, Winter J, Zaganelli S, Mahecic D, Perreten Lambert H, Ruberto FP, Nemir M, Wai T, Pedrazzini T *et al* (2021) Distinct fission signatures predict mitochondrial degradation or biogenesis. *Nature* 593: 435-439

Kolitsida P, Zhou J, Rackiewicz M, Nolic V, Dengjel J, Abeliovich H (2019) Phosphorylation of mitochondrial matrix proteins regulates their selective mitophagic degradation. *Proc Natl Acad Sci U S A* 116: 20517-20527

Korobova F, Gauvin TJ, Higgs HN (2014) A role for myosin II in mammalian mitochondrial fission. *Curr Biol* 24: 409-414

Korobova F, Ramabhadran V, Higgs HN (2013) An actin-dependent step in mitochondrial fission mediated by the ER-associated formin INF2. *Science* 339: 464-467

Kostic M, Katoshevski T, Sekler I (2018) Allosteric Regulation of NCLX by Mitochondrial Membrane Potential Links the Metabolic State and Ca(2+) Signaling in Mitochondria. *Cell Rep* 25: 3465-3475 e3464

Kostic M, Ludtmann MH, Bading H, Hershfinkel M, Steer E, Chu CT, Abramov AY, Sekler I (2015) PKA Phosphorylation of NCLX Reverses Mitochondrial Calcium Overload and Depolarization, Promoting Survival of PINK1-Deficient Dopaminergic Neurons. *Cell Rep* 13: 376-386

Kostic M, Sekler I (2019) Functional properties and mode of regulation of the mitochondrial Na(+)/Ca(2+) exchanger, NCLX. *Semin Cell Dev Biol* 94: 59-65

Kumar AV, Mills J, Lapierre LR (2022) Selective Autophagy Receptor p62/SQSTM1, a Pivotal Player in Stress and Aging. *Front Cell Dev Biol* 10: 793328

Labbe K, Murley A, Nunnari J (2014) Determinants and functions of mitochondrial behavior. *Annu Rev Cell Dev Biol* 30: 357-391

Lin Q, Dai Q, Meng H, Sun A, Wei J, Peng K, Childress C, Chen M, Shao G, Yang W (2017) The HECT E3 ubiquitin ligase NEDD4 interacts with and ubiquitylates SQSTM1 for inclusion body autophagy. *J Cell Sci* 130: 3839-3850

Lu K, Li P, Zhang M, Xing G, Li X, Zhou W, Bartlam M, Zhang L, Rao Z, He F (2011) Pivotal role of the C2 domain of the Smurf1 ubiquitin ligase in substrate selection. *J Biol Chem* 286: 16861-16870

MacVicar TD, Lane JD (2014) Impaired OMA1-dependent cleavage of OPA1 and reduced DRP1 fission activity combine to prevent mitophagy in cells that are dependent on oxidative phosphorylation. *J Cell Sci* 127: 2313-2325

Martinez M, Martinez NA, Silva WI (2017) Measurement of the Intracellular Calcium Concentration with Fura-2 AM Using a Fluorescence Plate Reader. *Bio Protoc* 7: e2411

Montero M, Alonso MT, Albillos A, Garcia-Sancho J, Alvarez J (2001) Mitochondrial Ca(2+)-induced Ca(2+) release mediated by the Ca(2+) uniporter. *Mol Biol Cell* 12: 63-71

Mourier A, Motori E, Brandt T, Lagouge M, Atanassov I, Galinier A, Rappl G, Brodesser S, Hultenby K, Dieterich C *et al* (2015) Mitofusin 2 is required to maintain mitochondrial coenzyme Q levels. *J Cell Biol* 208: 429-442

Narendra D, Tanaka A, Suen DF, Youle RJ (2008) Parkin is recruited selectively to impaired mitochondria and promotes their autophagy. *J Cell Biol* 183: 795-803

Numata M, Petrecca K, Lake N, Orlowski J (1998) Identification of a mitochondrial Na+/H+ exchanger. *J Biol Chem* 273: 6951-6959

Palty R, Silverman WF, Hershfinkel M, Caporale T, Sensi SL, Parnis J, Nolte C, Fishman D, Shoshan-Barmatz V, Herrmann S *et al* (2010) NCLX is an essential component of mitochondrial Na+/Ca2+ exchange. *Proc Natl Acad Sci U S A* 107: 436-441

Peng H, Yang J, Li G, You Q, Han W, Li T, Gao D, Xie X, Lee BH, Du J *et al* (2017) Ubiquitylation of p62/sequestosome1 activates its autophagy receptor function and controls selective autophagy upon ubiquitin stress. *Cell Res* 27: 657-674

Peng W, Wong YC, Krainc D (2020) Mitochondria-lysosome contacts regulate mitochondrial Ca(2+) dynamics via lysosomal TRPML1. *Proc Natl Acad Sci U S A* 117: 19266-19275

Plant PJ, Lafont F, Lecat S, Verkade P, Simons K, Rotin D (2000) Apical membrane targeting of Nedd4 is mediated by an association of its C2 domain with annexin XIIIb. *J Cell Biol* 149: 1473-1484

Quiros PM, Ramsay AJ, Sala D, Fernandez-Vizarra E, Rodriguez F, Peinado JR, Fernandez-Garcia MS, Vega JA, Enriquez JA, Zorzano A *et al* (2012) Loss of mitochondrial protease OMA1 alters processing of the GTPase OPA1 and causes obesity and defective thermogenesis in mice. *The EMBO journal* 31: 2117-2133

Rainbolt TK, Lebeau J, Puchades C, Wiseman RL (2016) Reciprocal Degradation of YME1L and OMA1 Adapts Mitochondrial Proteolytic Activity during Stress. *Cell Rep* 14: 2041-2049

Sadhu L, Tsopoulidis N, Hasanuzzaman M, Laketa V, Way M, Fackler OT (2023) ARPC5 isoforms and their regulation by calcium-calmodulin-N-WASP drive distinct Arp2/3-dependent actin remodeling events in CD4 T cells. *Elife* 12

Saha B, Olsvik H, Williams GL, Oh S, Evjen G, Sjottem E, Mandell MA (2024) TBK1 is ubiquitinated by TRIM5alpha to assemble mitophagy machinery. *Cell Rep* 43: 114294

Samanta K, Mirams GR, Parekh AB (2018) Sequential forward and reverse transport of the Na(+) Ca(2+) exchanger generates Ca(2+) oscillations within mitochondria. *Nat Commun* 9: 156

Santel A, Fuller MT (2001) Control of mitochondrial morphology by a human mitofusin. *J Cell Sci* 114: 867-874

Schuettpelz J, Janer A, Antonicka H, Shoubridge EA (2023) The role of the mitochondrial outer membrane protein SLC25A46 in mitochondrial fission and fusion. *Life Sci Alliance* 6

Sebastian D, Hernandez-Alvarez MI, Segales J, Sorianello E, Munoz JP, Sala D, Waget A, Liesa M, Paz JC, Gopalacharyulu P *et al* (2012) Mitofusin 2 (Mfn2) links mitochondrial and endoplasmic reticulum function with insulin signaling and is essential for normal glucose homeostasis. *Proc Natl Acad Sci U S A* 109: 5523-5528

Steffen J, Vashisht AA, Wan J, Jen JC, Claypool SM, Wohlschlegel JA, Koehler CM (2017) Rapid degradation of mutant SLC25A46 by the ubiquitin-proteasome system results in MFN1/2-mediated hyperfusion of mitochondria. *Mol Biol Cell* 28: 600-612

Stepp WL, Tortarolo G, Landoni JC, Durmus EB, Rodriguez Alvarez SN, Douglass KM, Weigert M, Manley S (2026) Smart hybrid microscopy for cell-friendly detection of rare events. *Nat Commun*

Sun A, Wei J, Childress C, Shaw JHt, Peng K, Shao G, Yang W, Lin Q (2017) The E3 ubiquitin ligase NEDD4 is an LC3-interactive protein and regulates autophagy. *Autophagy* 13: 522-537

Taha M, Assali EA, Ben-Kasus Nissim T, Stutzmann GE, Shirihai OS, Hershfinkel M, Sekler I (2024) NCLX controls hepatic mitochondrial Ca(2+) extrusion and couples hormone-mediated mitochondrial Ca(2+) oscillations with gluconeogenesis. *Mol Metab* 87: 101982

Tondera D, Grandemange S, Jourdain A, Karbowski M, Mattenberger Y, Herzig S, Da Cruz S, Clerc P, Raschke I, Merkwirth C *et al* (2009) SLP-2 is required for stress-induced mitochondrial hyperfusion. *EMBO J* 28: 1589-1600

Toyama EQ, Herzig S, Courchet J, Lewis TL, Jr., Loson OC, Hellberg K, Young NP, Chen H, Polleux F, Chan DC *et al* (2016) Metabolism. AMP-activated protein kinase mediates mitochondrial fission in response to energy stress. *Science* 351: 275-281

Twig G, Elorza A, Molina AJ, Mohamed H, Wikstrom JD, Walzer G, Stiles L, Haigh SE, Katz S, Las G *et al* (2008) Fission and selective fusion govern mitochondrial segregation and elimination by autophagy. *EMBO J* 27: 433-446

Verhoeven K, Claeys KG, Zuchner S, Schroder JM, Weis J, Ceuterick C, Jordanova A, Nelis E, De Vriendt E, Van Hul M *et al* (2006) MFN2 mutation distribution and genotype/phenotype correlation in Charcot-Marie-Tooth type 2. *Brain : a journal of neurology* 129: 2093-2102

Vetralla M, Wischhof L, Kahsay A, Cadenelli V, Scifo E, Xie B, Sbrissa M, Habert MS, Ehninger D, Rizzuto R *et al* (2025) TMEM65-dependent Ca2+ extrusion safeguards mitochondrial homeostasis. *Nat Commun*

Wang N, Wang X, Lan B, Gao Y, Cai Y (2025a) DRP1, fission and apoptosis. *Cell Death Discov* 11: 150

Wang Q, Sun Y, Li TY, Auwerx J (2026) Mitophagy in the pathogenesis and management of disease. *Cell Res* 36: 11-37

Wang R, Wang J, Yu J, Li Z, Zhang M, Chen Y, Liu F, Jiang D, Guo J, Li X *et al* (2025b) Mfn2 regulates calcium homeostasis and suppresses PASMCs proliferation via interaction with IP3R3 to mitigate pulmonary arterial hypertension. *J Transl Med* 23: 366

Wilkins HM, Troutwine BR, Menta BW, Manley SJ, Strope TA, Lysaker CR, Swerdlow RH (2022) Mitochondrial Membrane Potential Influences Amyloid-beta Protein Precursor Localization and Amyloid-beta Secretion. *J Alzheimers Dis* 85: 381-394

Wong YC, Kim S, Peng W, Krainc D (2019) Regulation and Function of Mitochondria-Lysosome Membrane Contact Sites in Cellular Homeostasis. *Trends Cell Biol* 29: 500-513

Wong YC, Ysselstein D, Krainc D (2018) Mitochondria-lysosome contacts regulate mitochondrial fission via RAB7 GTP hydrolysis. *Nature* 554: 382-386

Xiao S, Yu Y, Liao M, Song D, Xu X, Tian L, Zhang R, Lyu H, Guo D, Zhang Q *et al* (2025) Post-Translational Modification of p62: Roles and Regulations in Autophagy. *Cells* 14

Xu S, Wang P, Zhang H, Gong G, Gutierrez Cortes N, Zhu W, Yoon Y, Tian R, Wang W (2016) CaMKII induces permeability transition through Drp1 phosphorylation during chronic beta-AR stimulation. *Nat Commun* 7: 13189

Yang JF, Xing X, Luo L, Zhou XW, Feng JX, Huang KB, Liu H, Jin S, Liu YN, Zhang SH *et al* (2023) Mitochondria-ER contact mediated by MFN2-SERCA2 interaction supports CD8(+) T cell metabolic fitness and function in tumors. *Sci Immunol* 8: eabq2424

Youle RJ, van der Bliek AM (2012) Mitochondrial fission, fusion, and stress. *Science* 337: 1062-1065

Zaninello M, Palikaras K, Sotiriou A, Tavernarakis N, Scorrano L (2022) Sustained intracellular calcium rise mediates neuronal mitophagy in models of autosomal dominant optic atrophy. *Cell Death Differ* 29: 167-177

Zhang J, Wang X, Vikash V, Ye Q, Wu D, Liu Y, Dong W (2016) ROS and ROS-Mediated Cellular Signaling. *Oxid Med Cell Longev* 2016: 4350965

Zhang JL, Chang YC, Lai PH, Yeh HI, Tsai CW, Huang YL, Liu TY, Lee IC, Foulon N, Xu Y *et al* (2025) TMEM65 functions as the mitochondrial Na(+)/Ca(2+) exchanger. *Nat Cell Biol* 27: 1301-1310

Zhou W, Chen KH, Cao W, Zeng J, Liao H, Zhao L, Guo X (2010) Mutation of the protein kinase A phosphorylation site influences the anti-proliferative activity of mitofusin 2. *Atherosclerosis* 211: 216-223

Zuchner S, Mersiyanova IV, Muglia M, Bissar-Tadmouri N, Rochelle J, Dadali EL, Zappia M, Nelis E, Patitucci A, Senderek J *et al* (2004) Mutations in the mitochondrial GTPase mitofusin 2 cause Charcot-Marie-Tooth neuropathy type 2A. *Nat Genet* 36: 449-451

Figure Legends

Fig. 1. PXA-induced mitochondrial constrictions are controlled by Mitofusins. (**A**) Tom20 (red) and Hsp60 (green) immunofluorescence of MEFs with genotypes as indicated and 30 min treatments at 37 °C with DMSO or 10 μM PXA. Boxed areas were enlarged to show morphological changes. Scale bar is 10 μm. (**B**) Similar images with Drp1 KO and Drp1-Mfn2 DKO HeLa cells. (**C, D**) Manders' coefficients of Tom20 and Hsp60 colocalization to quantify matrix contraction. Averages ± SD from three independent experiments (50 images per condition) analyzed by one-way ANOVA with Tukey's HSD post hoc test.

Fig. 2. Mfn2 regulates mitochondrial Ca^{2+} efflux and membrane potential through NCLX. (**A**) Tracings of mitochondrial matrix Ca^{2+} detected with matrix3mt-R-CEPIA in HeLa cells with genotypes as indicated. Baseline (Fo) was established using 60-sec tracings. Ca^{2+} release was induced with 10 μM PXA, followed by 600 sec of further recording. Where indicated, cells were pre-incubated for 30 min at 37 °C with 10 μM CGP37157. (**B**) Relative fluorescence (F/Fo) at 400 sec, reflecting changes in mitochondrial Ca^{2+} levels. (**C**) Effects of PXA on mitochondrial membrane potential (ΔΨ) in Drp1 KO HeLa cells stained with 25 nM TMRM. Where indicated, cells were preincubated for 30 min with 100 nM BIX (NHE1 inhibitor) or 10 μM CGP37157 (NCLX inhibitor). Baselines and tracings after perfusion with or without 10 μM PXA were obtained as in panel A. Perfusion with 10 μM CCCP was used as a control for dissipation of ΔΨ. (**D**) Averages of F/Fo were determined at 300 seconds after perfusion. (**E)** Cartoon to illustrate how ΔΨ is reduced by Na^+/H^+ exchange through NHE1 when Ca^{2+} efflux is induced by PXA. (**F,G**) Tracings and histogram of TMRM fluorescence with Drp1-Mfn2 DKO cells instead of Drp1 KO cells. Throughout, averages with SD are shown with significance analyzed by one-way ANOVA with Tukey's HSD post hoc test.

Fig. 3. PXA targets Mitofusins and induces interactions between Mfn2 and NCLX. (**A**) CETSA to determine the target of PXA. Dodecyl maltoside extracts from cells with the indicated genotypes were

incubated with DMSO or 1uM PXA and subjected to heat denaturation for 3 min at the indicated temperatures, followed by removal of denatured proteins by centrifugation and western blot analysis of the supernatants. The upper panel was made with Drp1-Mfn2 DKO cells that stably express exogenous Mfn2-FLAG, while the lower two sets of blots were made with endogenous proteins. (**B**) Band intensities determined with densitometric scans of blots as shown in panel A. The intensities were normalized to the bands at 45 or 50°C, showing averages with SD from 3 independent experiments. (**C**) Co-immunoprecipitation (coIP) of endogenous NCLX and SLC25A46 with Mfn2-FLAG using FLAG antibody attached to beads. Cells grown under glycolytic conditions (Gly) were treated for 30 min with DMSO, 10 μM each of PXA, CCCP or CGP37157, or grown under respiring conditions (galactose). These cells were incubated with DSP cross-linker and subjected to coIP, followed by western blot analysis. Actin was used as a loading control. (**D**) Densitometry of the NCLX coIPs, normalized to the levels of Mfn2 for each condition. Averages of 5 independent experiments are shown with SD and results of an unpaired Student's t-test. (**E**) Densitometry of SLC25A46 coIPs as described for NCLX in panel D. Averages of 3 independent experiments with SD and results of an unpaired Student's t-test are shown. (**F**) CoIP of Calnexin with Mfn2-FLAG after treatment with PXA under glycolytic conditions as described in panel C. (**G**) Densitometry of Calnexin coIP with Mfn2-FLAG as in panels D and E. Averages of 3 independent experiments with SD and results of an unpaired Student's t-test are shown. (**H**) PLA of Mfn2-myc and NCLX-HA (red spots) in glycolytic Drp1 KO MEFs treated for 30 min with DMSO or 10 μM PXA. Mitochondria were detected by immunofluorescence with a chicken antibody against Hsp60 (green). The size marker is 10 μm. (**I**) Average numbers of PLA spots per cell from 3 independent experiments with SD and results of an unpaired Student's t-test are shown. PLA spots in 35 cells were counted for each experiment.

Fig. 4. Stress-induced mitochondrial Ca^{2+} release is regulated by a complex of Mfn2 and NCLX. (**A**) Tracings of mitochondrial Ca^{2+} fluorescence detected with matrix-3mt-CEPIA in HeLa cells with genotypes as indicated. Measurements were as described in Fig. 2A. Where indicated, cells were pre-incubated for 30 min at 37 °C with 10 μM CGP37157. (**B**) Quantification of mitochondrial Ca^{2+} levels, expressed as F/Fo at 400 sec after oligomycin treatment, as in Fig. 2B.(**C, D**) Tracings and histograms of mitochondrial matrix Ca^{2+}, as in panels A and B but treated with 50 μM mitoPQ. (**E**) Tracings of cytosolic Ca^{2+} induced in respiring Hela cells with 10 μM oligomycin and detected with Calbryte-520 AM. Where indicated, cells were pre-incubated for 30 min with 10 μM CGP37157. (**F**) Changes in cytosolic Ca^{2+} levels reflected by the relative fluorescence (F/Fo) at 600 sec. (**G,H**) Tracings and histograms of cytosolic Ca^{2+} levels as in panels E and F but induced with 50 μM mitoPQ. (**I**) PLA of Mfn2-myc and NCLX-HA (red spots) in respiring Drp1 KO MEFs treated with DMSO, 10 μM oligomycin, or 50 μM mitoPQ. Mitochondria were detected by immunofluorescence with chicken Hsp60 antibody (green). (**J**) Number of PLA spots per cell, averaged across 25 cells for each condition in three rounds of experiments. (**K**) PLA of Mfn2-myc and endogenous SERCA2 (red spots) in respiring Drp1 KO MEFs treated and quantified as in panel J. (**L**) Numbers of PLA spots per cell analyzed as described in panel J. (**M,N**) PLA of Mfn2-myc and endogenous SERCA2 (red spots) in respiring Drp1 KO MEFs treated and quantified as in panel J. The size markers in panels I, K and M are 10 μm. Throughout, averages are shown with SD and significance was determined with one-Way ANOVA with Tukey's HSD post hoc test.

Fig. 5. SLC25A46 is required for Mfn2-NCLX interactions and stress-induced Ca^{2+} release. (**A**) Tracings of mitochondrial matrix Ca^{2+} in respiring HeLa cells, detected as in Fig. 2A, but induced with 10 μM oligomycin or 50 μM mitoPQ, and in cells that were transfected with siRNA for SLC25A46. (**B**) Changes in mitochondrial Ca^{2+} levels reflected by the relative fluorescence (F/Fo) at 600 sec. (**C**) PLA of Mfn2-myc and NCLX-HA (red spots) in respiring Drp1 KO or SLC25A46 Drp1 KO MEFs treated with DMSO or 10 μM oligomycin, or 50 μM mitoPQ. Mitochondria were detected with chicken Tom20 antibody (green). The size marker is 10 μm. (**D**) Number of PLA spots for Mfn2-myc and NCLX-HA per cell, averaged across 25 cells for each condition in three rounds of experiments. (**E**) Western blots showing coIP of NCLX and SLC25A46 with Mfn2-FLAG in WT and SLC25A45 KO cells. (**F**) PLA of SLC25A46-

myc and NCLX-HA (red spots) in respiring Drp1 KO MEFs treated for 30 min with DMSO, 10 μM oligomycin, or 10 μM CGP37157. Mitochondria were detected with chicken Tom20 antibody (green). The size marker is 10 μm. (**G**) Number of PLA spots for SLC25A46-myc and NCLX-HA per cell, averaged across 25 cells for each condition in three rounds of experiments.

Fig. 6. Mitochondrial ROS activation of Oma1 and PKA triggers Ca^{2+} release. (**A**) Immunofluorescence of WT and Oma1 KO HeLa cells treated for 30 min with DMSO or 10 μM oligomycin in respiring conditions. Merged images show Tomm20 (red) and Hsp60 (green), while the black and white images show Tomm20 labeling separately. Scale bar is 10 μm. (**B**) Aspect ratios of mitochondrial outer membranes (Tom20) under the conditions for panel B. Aspect ratios were determined for each condition with mitochondria in 25 cells per experiment in 3 independent experiments with SD and results of a one-way ANOVA. (**C**) PLA of Mfn2-myc and NCLX-HA (red spots) in WT and Oma1 KO HeLa cells grown under respiring conditions and treated for 30 min with DMSO or 10 μM Oligomycin. Mitochondria were detected by immunofluorescence with chicken Hsp60 antibody (green). Scale bar is 10 μm. (**D**) Numbers of PLA spots per cells treated with DMSO or oligomycin from 3 independent experiments with SD and results of a one-way ANOVA. (**E**) Tracings of mitochondrial matrix Ca^{2+}, detected as in Fig. 2A, in WT and Oma1 KO HeLa cells grown under respiring conditions and treated with 10 μM oligomycin. Where indicated with CGP, cells were preincubated for 30 min at 37 °C with 10 μM CGP37157. (**F**) Changes in mitochondrial Ca^{2+} levels are reflected by the relative fluorescence (F/Fo) at 400 sec. Averages are shown with SD, and significance is determined with one-way ANOVA. (**G**) Tracings of mitochondrial matrix Ca^{2+} in respiring HeLa cells, detected as in Fig. 2A, but induced with 10 μM oligomycin or 50 μM mitoPQ, with or without pretreatment for 30 min with 10 μM H89 (PKA inhibitor). (**H**) Relative fluorescence (F/Fo) at 600 sec, reflecting changes in mitochondrial Ca^{2+} levels. (**I**) Tracings of mitochondrial matrix Ca^{2+} in respiring HeLa cells, detected as in Fig. 2A, but induced with 10 μM oligomycin or 50 μM mitoPQ, in NCLX KO cells that stably express exogenously introduced wt NCLX-HA or NCLX(S258A)-HA. (**J**) Quantification of mitochondrial Ca^{2+} efflux rates of F/Fo. Averages are shown with SD and significance was determined with one-way ANOVA with Tukey's HSD post hoc test.

Fig. 7. ROS-induced mitochondrial Ca^{2+} release promotes mitophagy by activating NEDD4-1. (**A**) Representative live images of WT SHY-5Y cells that stably express mitoQC (Fis1-mCherry-GFP) introduced with a lentivirus. Cells were pre-incubated with 10 μM CGP37157 or 5 mM NAC for 30 min at 37 °C and treated for 10 μM oligomycin for 30 min at 37 °C. Scale bar is 10 μm. (**B**) Quantification of red puncta per cell from 3 independent experiments with SD and results of one-Way ANOVA. (**C, D**) SHY-5Y cells were pre-incubated as in panels A and B, but then treated for 30 min with 50 μM mitoPQ. (**E**) HeLa cells that stably express mitoQC were transiently transfected with a Parkin construct (mock) or with Parkin and NEDD4-1 constructs (NEDD4), followed by preincubations with CGP37157 or NAC and treatments with oligomycin and mitoPQ as in panels A-D. (**F**) Quantification of red puncta per cell from 3 independent experiments with SD and results of one-Way ANOVA. (**G**) Proposed pathway linking ROS-induced mitochondrial Ca^{2+} release to cytosolic Ca^{2+} dependent activation of mitophagy.

Fig. S1. Western blots of knockout cells and scatterplots for immunofluorescence analysis. (**A**) Western blot confirmation of knockouts used for IF experiments. Actin and tubulin are loading controls. (**B**) Scatter plots of Hsp60 and Tom20 immunofluorescence with Drp1 KO cells treated with or without 10 μM PXA to illustrate colocalization as an indicator of mitochondrial matrix constrictions. Matrix and outer membrane markers largely colocalize in cells treated with DMSO, as evidenced by a linear relation in the scatterplot, whereas they separate when treated with PXA, resulting in a random distribution in the scatterplot.

Fig. S2. Western blots showing NCLX knockout in HeLa cells, PXA-induced Ca^{2+} release detected with Rhod-2AM, and plots of mitochondrial membrane potential affected by Ca^{2+} release. (**A**) Validation of NCLX KO in HeLa cells with a western blot of extracts from NCLX KO cells, flanked by extracts from WT and NCLX siRNA cells. The NCLX antibody cross-reacts with another protein at around 57 kDa, but a band corresponding to the predicted MW of NCLX (64 kDa, shown with an arrow) is present in WT cells, absent from NCLX KO cells, and greatly diminished in NCLX siRNA cells. (**B**) Time course of soluble mitochondrial Ca^{2+} levels in MEFs detected with Rhod-2 AM, upon treatment with 10 μM PXA. Drp1 KO MEFs were transduced with scrambled siRNA (SCR), NCLX siRNA, or pretreated for 30 min with 10 μM CGP37157. Mfn2-Drp1 DKO MEFs were also tested. (**C, D**) Quantification of mitochondrial Ca^{2+} levels detected with Rhod-2 AM as in panel B, showing induced and basal levels. (**E**) Tracing of mitochondrial Ca^{2+} levels in HeLa cells induced by 10 μM CCCP and detected with matrix-3mt-CEPIA as in Fig. 2A, showing that CCCP induces Ca^{2+} release independent of NCLX function. (**F**) Quantification of mitochondrial Ca^{2+} levels after CCCP treatment. Throughout, averages are shown with SD and significance was determined with one-way ANOVA with Tukey's HSD post hoc test.

Fig. S3. Verification that Mfn2-flag and Mfn2-myc tagged proteins are functional. (**A**) Fluorescence images showing that stable transfection with tagged Mfn2 constructs (Mfn2-FLAG or Mfn2-myc) restores filamentous mitochondrial morphology in Mfn2 KO MEFs. Mitochondria were detected with mito-GFP. Scale bar is 10 μm. (**B**) Identification of NCLX band in MEF extracts under conditions for CETSA experiments. This was necessary because the cross-reactivity observed with the available NCLX antibody changes with different solubilization conditions (see westerns with Laemmli sample buffer in HeLa cells (Fig. S2) versus dodecyl maltoside for the MEFs used for CETSA (Fig. 3). In both cases, NCLX was identified by the absence of a 64 kDa band in KO or siRNA cells, which is the predicted MW of NCLX. (**C**) Example of CETSA blot without drugs, but with extracts from WT and NCLX KO MEFs to show the stability over a range of temperatures and positive identification of the NCLX band by comparing with extracts from KO cells. (**D**) PLA of Mfn2-myc and NCLX-HA (red spots) in glycolytic Drp1 KO MEFs treated with DMSO. In this case mitochondria were detected by immunofluorescence with an antibody against a mitochondrial outer membrane protein (rabbit Tom20 antibody, green), showing that the spots are outer membrane tubules. Size marker is 10 μm.

Fig. S4. Mitochondrial ROS, Ca^{2+} release and membrane potential in different mutant HeLa cells. (**A**) Mitochondrial ROS detected with mitoSOX and expressed as corrected total cell fluorescence (CTCF) values. ROS was induced by oligomycin or mitoPQ, and as a control, quenched with NAC. ROS was detected by incubating WT HeLa cells for 30 min with 5 μM MitoSOX, with or without 30 min pre-treatment with 2 mM NAC. After this incubation, cells were washed with PBS and destained for 30 min during which cells were treated with 10 μM Oligomycin or 50 μM mitoPQ. CTCF was quantified per cell (25 cells per condition) across 3 independent experiments. (**B**) Tracings of mitochondrial matrix Ca^{2+} in respiring HeLa cells, detected as in Fig. 2A, but induced with 10 μM oligomycin or 50 μM mitoPQ, with or without pretreatment for 30 min with 2mM NAC. (**C**) Changes in mitochondrial Ca^{2+} levels reflected by the relative fluorescence (F/Fo) at 600 sec. (**D**) Effects of 50 μM or 100 μM mitoPQ on mitochondrial membrane potential (ΔΨ) determined with WT HeLa cells loaded with 25 nM TMRM. (**E**) Averages of F/Fo for TMRM determined at 400 sec after treatment with mitoPQ. (**F**) Validation of NCLX and Mfn2 siRNA knockdowns in HeLa cells with western blots. Vinculin is a loading control. (**G**) Tracings of mitochondrial matrix Ca^{2+} in respiring HeLa cells, detected as in Fig. 2A, but induced with 10 μM oligomycin. Where indicated, cells were pretreated for 30 min with 10 μM CGP37157 or transfected with siRNA. (**H**) Changes in mitochondrial Ca^{2+} levels reflected by the relative fluorescence (F/Fo) at 600 sec. (**I, J**) Tracings and histograms of mitochondrial matrix Ca^{2+}, as in panels A and B but treated with 50 μM mitoPQ. Throughout, averages are shown with SD and significance was determined with one-way ANOVA with Tukey's HSD post hoc test. (**K**) PLA of Mfn2-myc and NCLX-HA (red spots) in respiring Drp1 KO MEFs pre-treated for 30 min with 2mM NAC and then incubated for 30 min with DMSO, 10 μM oligomycin, or 50 μM mitoPQ. Mitochondria were detected with chicken Tom20 antibody (green). The

size marker is 10 μm. (**L**) Number of PLA spots for Mfn2-myc and NCLX-HA per cell, averaged across 25 cells for each condition in three rounds of experiments.

Fig. S5. Western blots to confirm SLC25A46 siRNA and knockout in HeLa cells and MEFs. (**A**) Validation of SLC25A46 siRNA knockdown in HeLa cells with western blots of extracts from WT and siRNA-treated cells. Vinculin is a loading control. (**B**) Validation of SLC25A46 KO in Drp1 KO MEFs. (**C**) Validation of SLC25A46 KO in HeLa cells. (**D**) Comparison of Mfn2-FLAG expression levels in WT and SLC25A46 KO HeLa cells. (**E**) Co-immunoprecipitation (coIP) of endogenous NCLX and Mfn2 with SLC25A46-HA using HA antibody beads. Drp1 KO MEFs grown under respiring conditions were treated for 30 min with DSMO, 10 μM oligomycin, or 50 μM mitoPQ, followed by incubation with BMH cross-linker, coIP and western blot analysis. (**F**) Densitometry of the NCLX coIP with SLC25A46, normalized to the levels of SLC25A46 for each condition. (**G**) Densitometry of Mfn2 coIP with SLC25A46, normalized to the levels of SLC25A46 for each condition. (**H**) Densitometry of SLC25A46 coIP with Mfn2, normalized to the levels of Mfn2 for each condition. Throughout, averages are shown with SD and significance was determined with one-way ANOVA with Tukey's HSD post hoc test.

Fig. S6. Oma1 cleavage of Opa1 controls Mfn2-NCLX association and Ca^{2+} release. (**A**) Western blot analysis of WT MEF cells treated with 10 μM Oligomycin for 0, 1, or 2 hours at 37 °C, probed with an Opa1 antibody. Tubulin was a loading control. (**B**) Western blot of wild type (WT) and Oma1 KO HeLa cells. Tubulin was a loading control. (**C**) Western blot of WT and Drp1-Opa1 DKO MEFs. (**D**) PLA of Mfn2-myc and NCLX-HA (red spots) in Drp1 KO and Drp1/Opa1 DKO MEFs grown as in panel D under respiring conditions and treated for 30 min with DMSO or 10 μM oligomycin. Mitochondria were detected with a chicken anti-Hsp60 antibody (green). Scale bar is 10 μm. (**E**) Numbers of PLA spots per cell in 25 cells treated with DMSO or 10 μM oligomycin from 3 independent experiments with SD and results of a one-way ANOVA. (H) Western blot showing stable expression of NCLX(WT)-HA and NCLX(S258A)-HA in HeLa NCLX KO cells. (**F**) Model depicting the replacement of Opa1 with NCLX in a complex with Mfn2 and SLC25A46, upon Oma1-mediated cleavage of Opa1. (**G**) Western blot of NCLX KO HeLa cells with stable expression of WT NCLX-HA or $NCLX^{S258A}$-HA. Vinculin is a loading control. (**H**) WT MEFs were treated with DMSO or 10 mM CGP37157 or 5 mM NAC for 30 min or 10 mM BAY-3827 for 2h at 37 °C followed by 10 mM Oligomycin or 50 mM mitoPQ for 30 min at 37 °C and labeled with Tom20 antibody for immunofluorescence. The size marker is 10 μm. (**I**) Aspect ratios of mitochondrial outer membrane (Tom20) under the conditions for panel a. Averages are shown for 3 independent experiments with SD and the results of one-Way ANOVA. Aspect ratios were determined for each condition with mitochondria in 25 cells per experiment.

Fig. S7. Effects of ROS-induced mitochondrial Ca^{2+} release on mitophagy and the effects of Ca^{2+} dependent E3 ubiquitin ligases on this process. (**A**) Representative live images of WT MEFs that stably express mitoQC (Fis1-mCherry-GFP) introduced with a lentivirus. Cells were pre-incubated with 10 μM CGP37157 or 5 mM NAC for 30 min at 37 °C and treated for 10 μM oligomycin for 30 min at 37 °C. Scale bar is 10 μm. (**B**) Quantification of red puncta per cell from 3 independent experiments with SD and results of one-Way ANOVA with Tukey's HSD post hoc test. (**C**) Live cell images of SH-SY5Y cells that express mitoQC, transfected with siRNA for genes as indicated, followed after 2 days by inducing mitophagy with 10 μM oligomycin for 30 min at 37 °C. Scale bar is 10 μm. (**D**) Quantification of red puncta per cell from 3 independent experiments with SD and results of one-Way ANOVA with Tukey's HSD post hoc test. (**E, F**) SH-SY5Y cells that express mitoQC were transfected with siRNA for the indicated genes as in panels C and D, but these were treated for for 30 min with 50 μM mitoPQ. (**G**) Western blot showing knockdown of NEDD4-1 with siRNA. (**H**) Western blot showing NEDD4-1 expression in cells transfected with an HA-tagged NEDD4-1 construct.

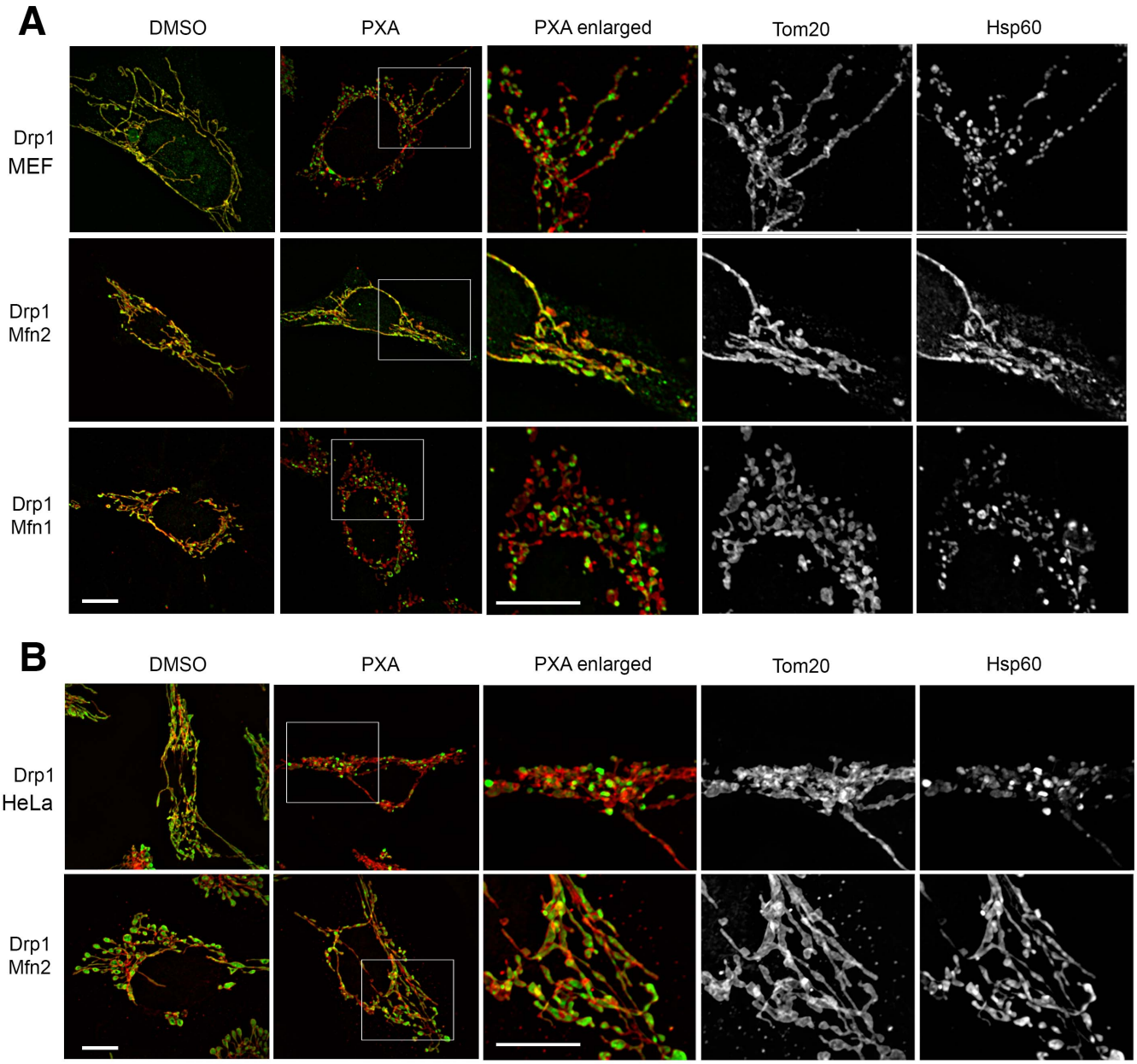
A
DMSO
PXA
PXA enlarged
Tom20
Hsp60
Drp1
MEF
Drp1
Mfn2
Drp1
Mfn1
B
DMSO
PXA
PXA enlarged
Tom20
Hsp60
Drp1
HeLa
Drp1
Mfn2
C
MEF
Manders' coefficient
1.0
0.5
***
***
DMSO
PXA
DMSO
PXA
DMSO
PXA
Drp1 KO
Drp1-Mfn2
Drp1-Mfn1
D
HeLa
Manders' coefficient
1.0
0.5
**
DMSO
PXA
DMSO
PXA
Drp1 KO
Drp1-Mfn2

Fig. 1

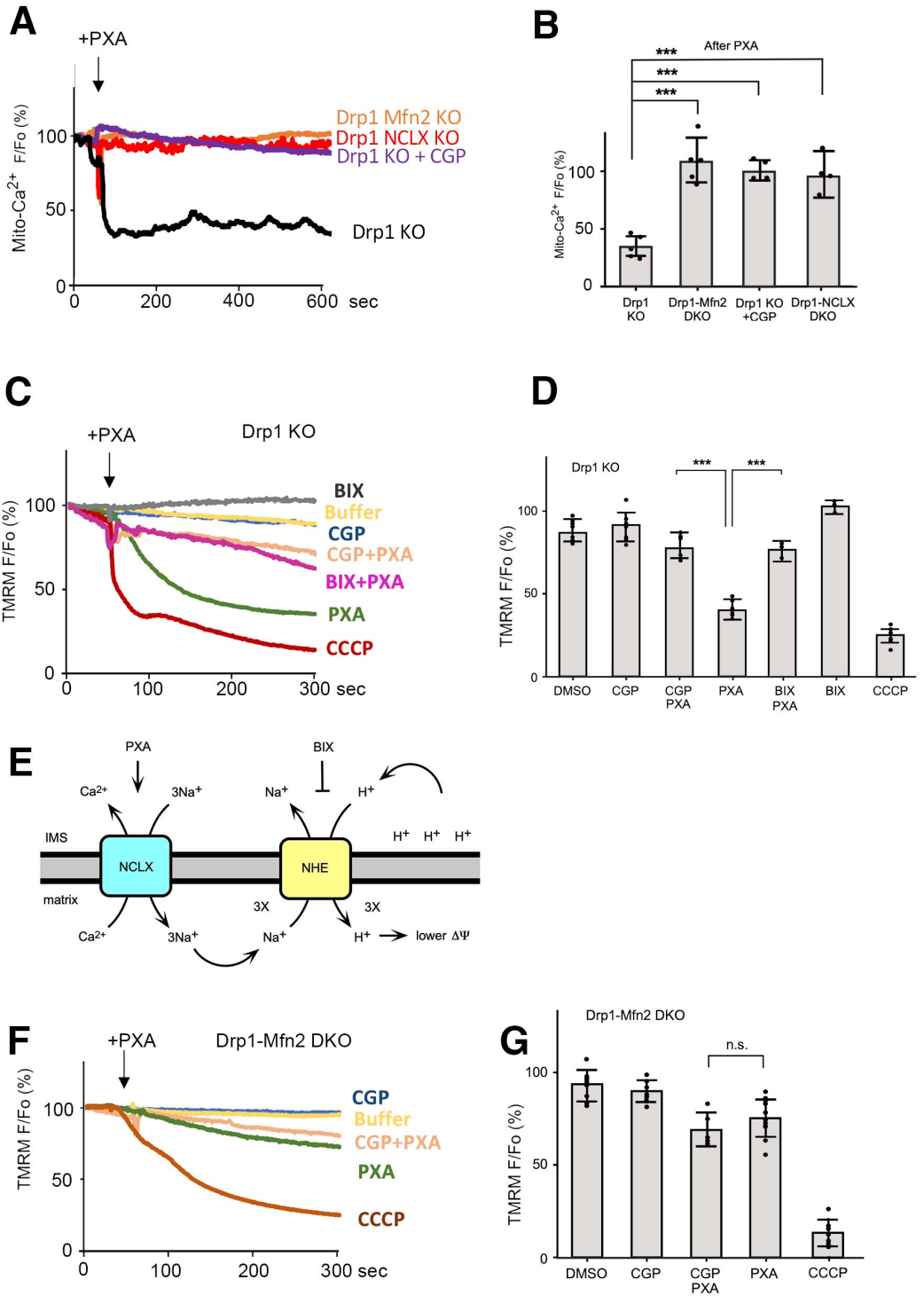
A
+PXA
Drp1 Mfn2 KO
Drp1 NCLX KO
Drp1 KO + CGP
Drp1 KO
Mito-Ca2+ F/Fo (%)
100
50
0
0
200
400
600 sec
B
After PXA
***
***
***
Mito-Ca2+ F/Fo (%)
100
50
0
Drp1 KO
Drp1-Mfn2 DKO
Drp1 KO +CGP
Drp1-NCLX DKO
C
+PXA
Drp1 KO
BIX
Buffer
CGP
CGP+PXA
BIX+PXA
PXA
CCCP
TMRM F/Fo (%)
100
50
0
0
100
200
300 sec
D
Drp1 KO
***
***
TMRM F/Fo (%)
100
50
0
DMSO
CGP
CGP PXA
PXA
BIX PXA
BIX
CCCP
E
PXA
BIX
Ca2+
3Na+
Na+
H+
IMS
matrix
NCLX
NHE
H+ H+ H+
3X
3X
Ca2+
3Na+
Na+
H+
lower ΔΨ
F
+PXA
Drp1-Mfn2 DKO
CGP
Buffer
CGP+PXA
PXA
CCCP
TMRM F/Fo (%)
100
50
0
0
100
200
300 sec
G
Drp1-Mfn2 DKO
n.s.
TMRM F/Fo (%)
100
50
0
DMSO
CGP
CGP PXA
PXA
CCCP

Fig. 2

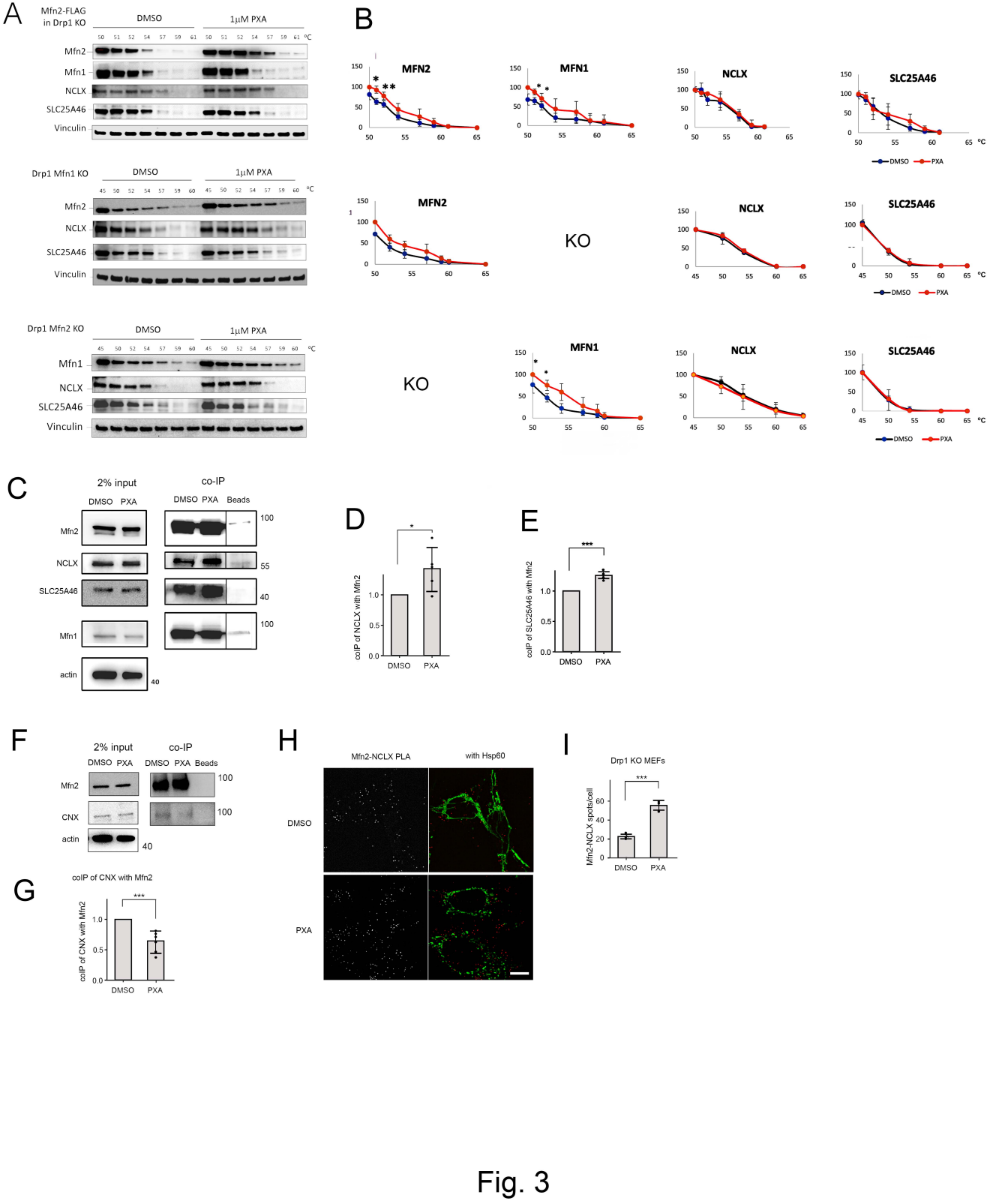
A
Mfn2-FLAG in Drp1 KO
DMSO
1μM PXA
Mfn2
Mfn1
NCLX
SLC25A46
Vinculin
Drp1 Mfn1 KO
Drp1 Mfn2 KO
B
MFN2
MFN1
NCLX
SLC25A46
KO
DMSO
PXA
°C
C
2% input
co-IP
Beads
actin
D
coIP of NCLX with Mfn2
E
coIP of SLC25A46 with Mfn2
F
CNX
G
coIP of CNX with Mfn2
H
Mfn2-NCLX PLA
with Hsp60
I
Drp1 KO MEFs
Mfn2-NCLX spots/cell

Fig. 3

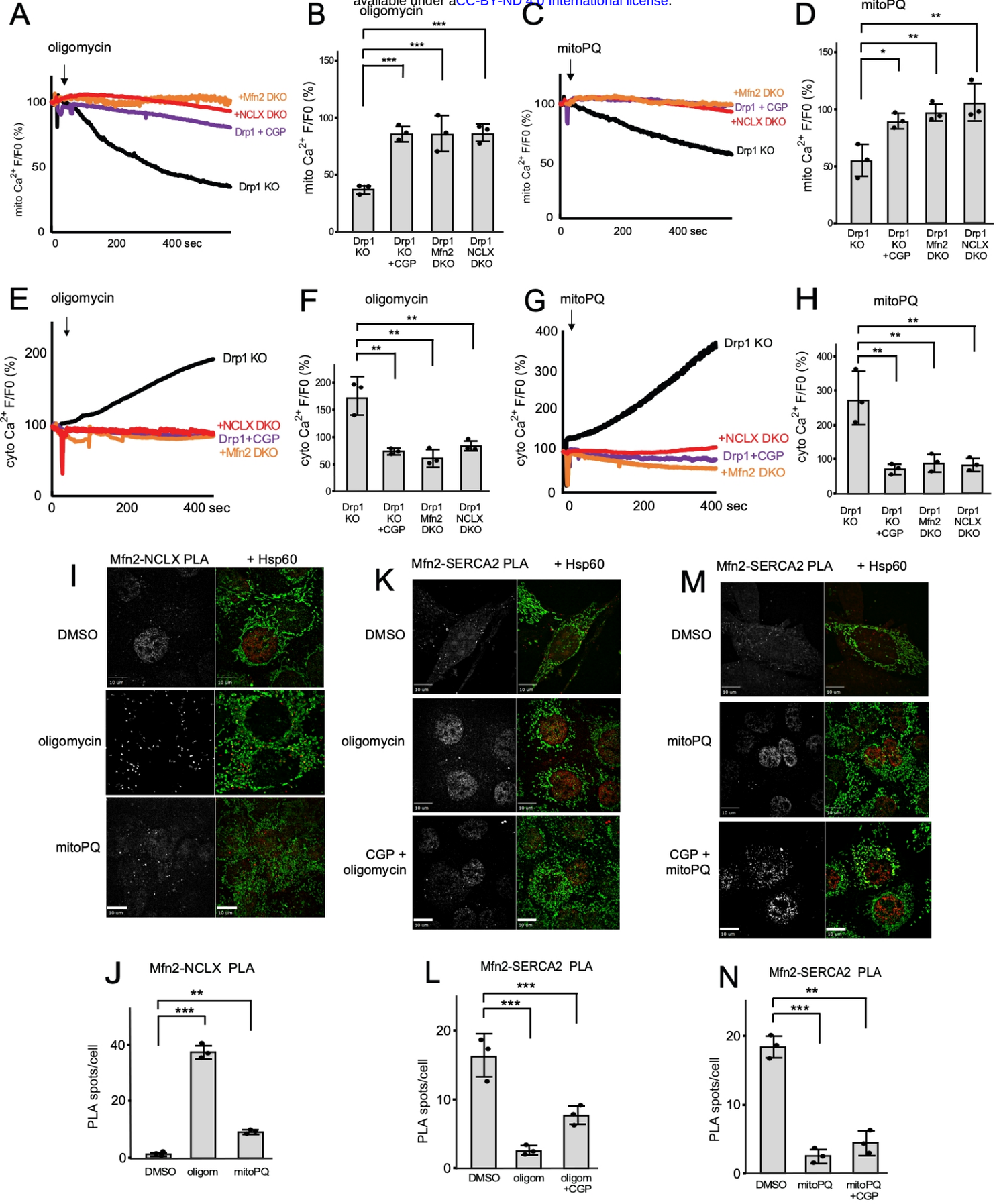

Fig. 4

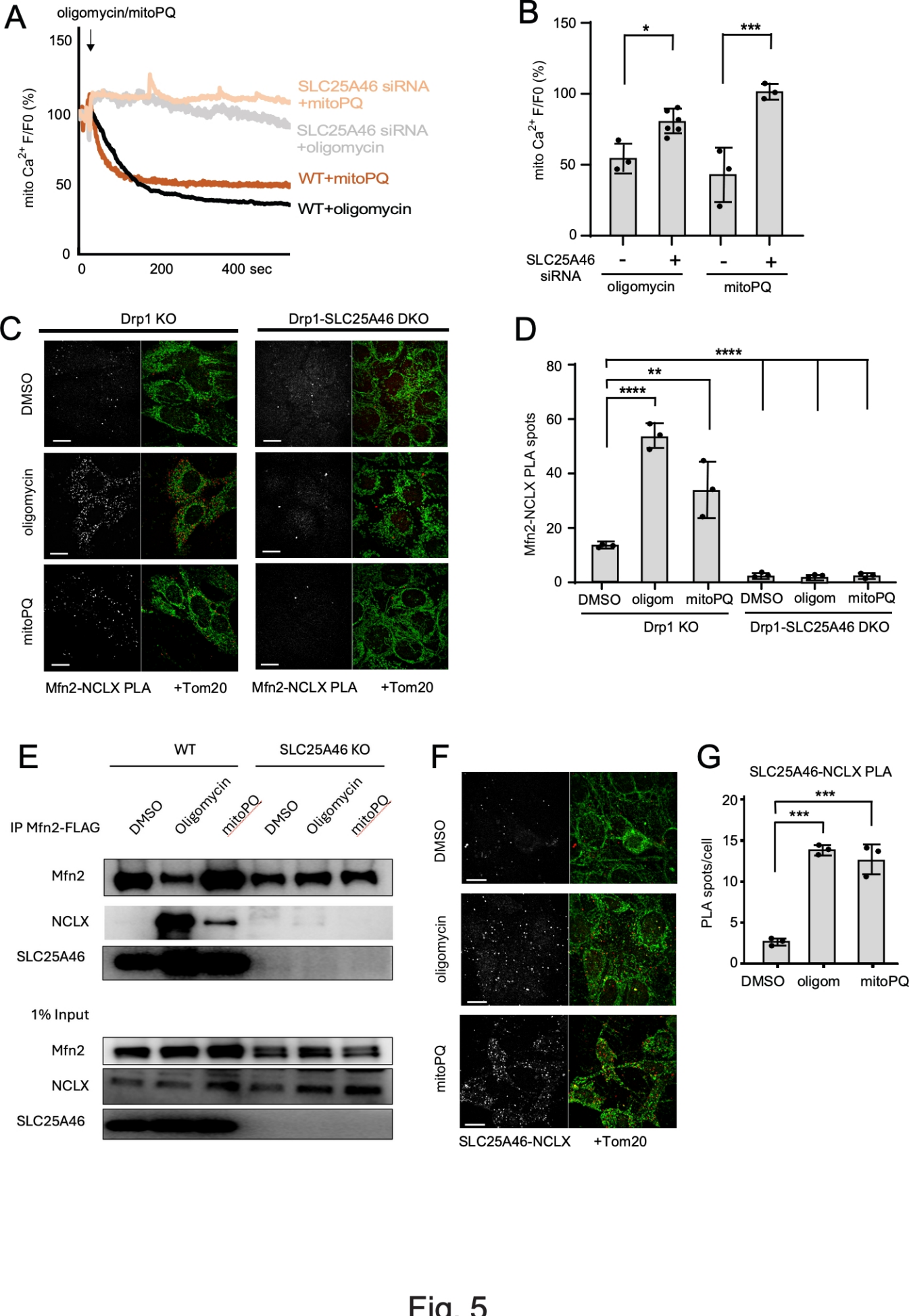
A
oligomycin/mitoPQ
mito Ca2+ F/F0 (%)
150
100
50
0
0
200
400 sec
SLC25A46 siRNA +mitoPQ
SLC25A46 siRNA +oligomycin
WT+mitoPQ
WT+oligomycin
B
mito Ca2+ F/F0 (%)
150
100
50
0
*
***
SLC25A46 siRNA
-
+
-
+
oligomycin
mitoPQ
C
Drp1 KO
Drp1-SLC25A46 DKO
DMSO
oligomycin
mitoPQ
Mfn2-NCLX PLA
+Tom20
Mfn2-NCLX PLA
+Tom20
D
Mfn2-NCLX PLA spots
80
60
40
20
0
****
**
****
DMSO
oligom
mitoPQ
DMSO
oligom
mitoPQ
Drp1 KO
Drp1-SLC25A46 DKO
E
WT
SLC25A46 KO
IP Mfn2-FLAG
DMSO
Oligomycin
mitoPQ
DMSO
Oligomycin
mitoPQ
Mfn2
NCLX
SLC25A46
1% Input
Mfn2
NCLX
SLC25A46
F
DMSO
oligomycin
mitoPQ
SLC25A46-NCLX
+Tom20
G
SLC25A46-NCLX PLA
PLA spots/cell
20
15
10
5
0
***
***
DMSO
oligom
mitoPQ

Fig. 5

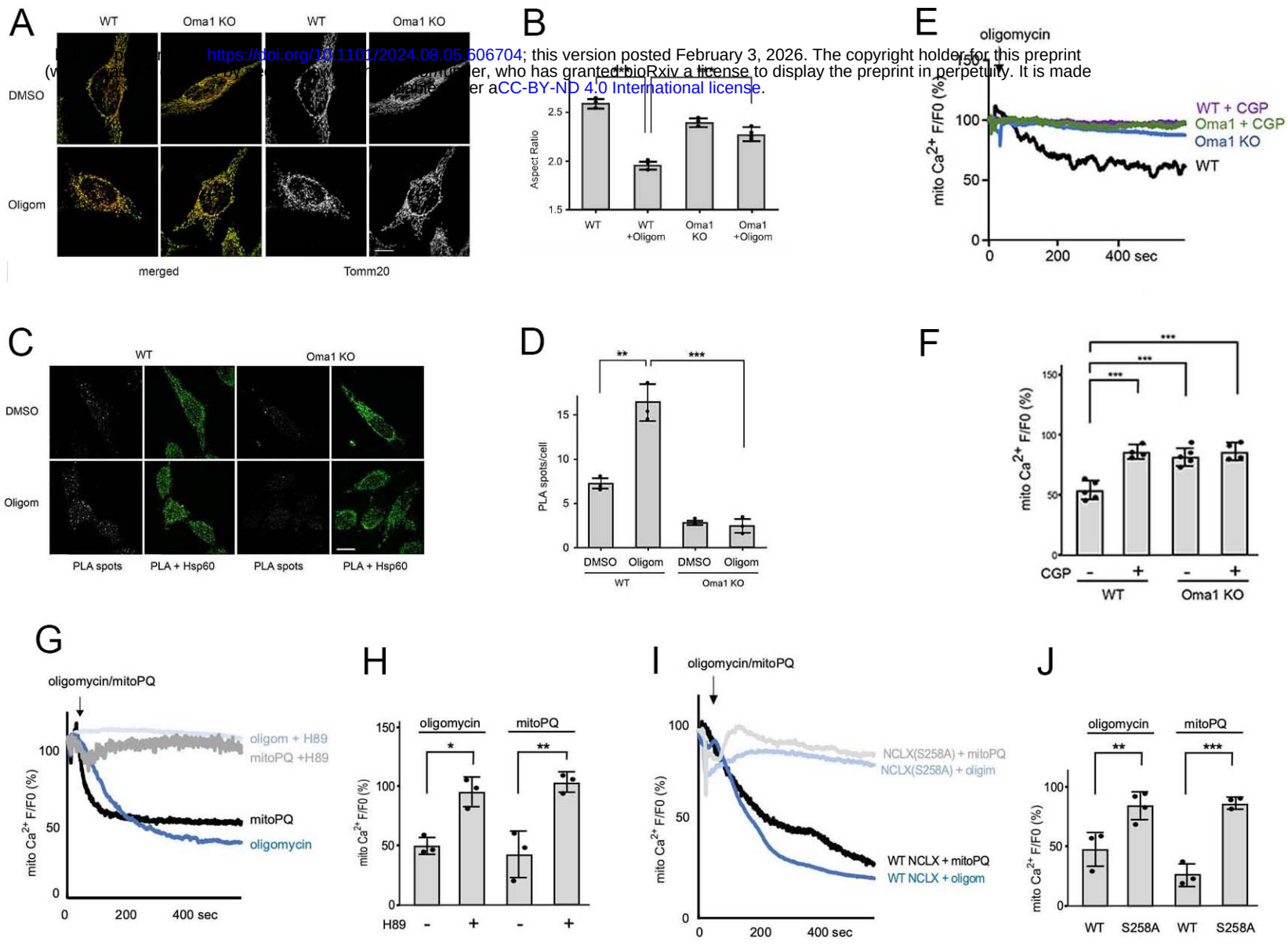

Fig. 6

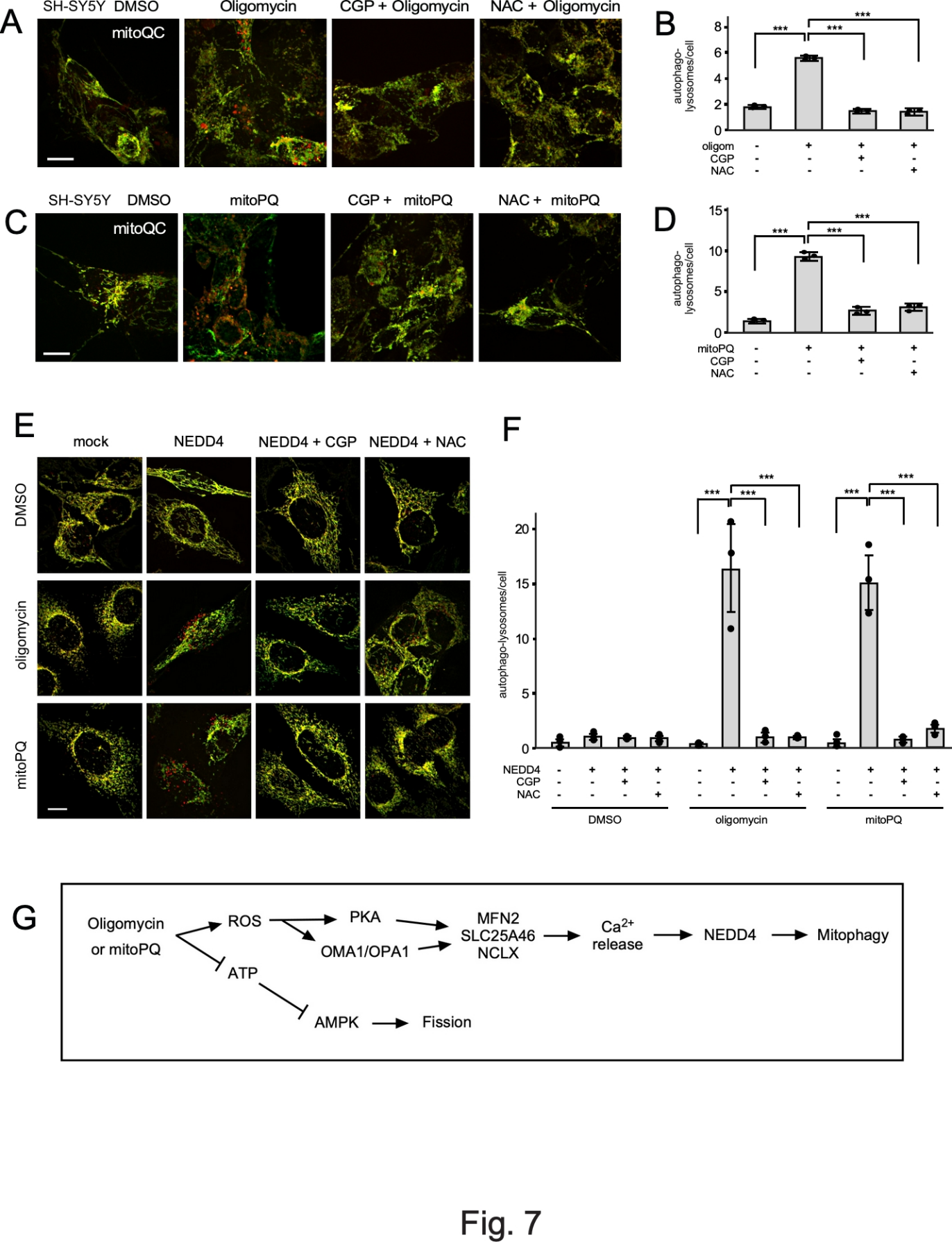
A
SH-SY5Y DMSO
Oligomycin
CGP + Oligomycin
NAC + Oligomycin
mitoQC
B
autophago-lysosomes/cell
oligom
CGP
NAC
C
SH-SY5Y DMSO
mitoPQ
CGP + mitoPQ
NAC + mitoPQ
mitoQC
D
autophago-lysosomes/cell
mitoPQ
CGP
NAC
E
mock
NEDD4
NEDD4 + CGP
NEDD4 + NAC
DMSO
oligomycin
mitoPQ
F
autophago-lysosomes/cell
NEDD4
CGP
NAC
DMSO
oligomycin
mitoPQ
G
Oligomycin
or mitoPQ
ROS
PKA
OMA1/OPA1
ATP
MFN2
SLC25A46
NCLX
Ca2+
release
NEDD4
Mitophagy
AMPK
Fission

Fig. 7

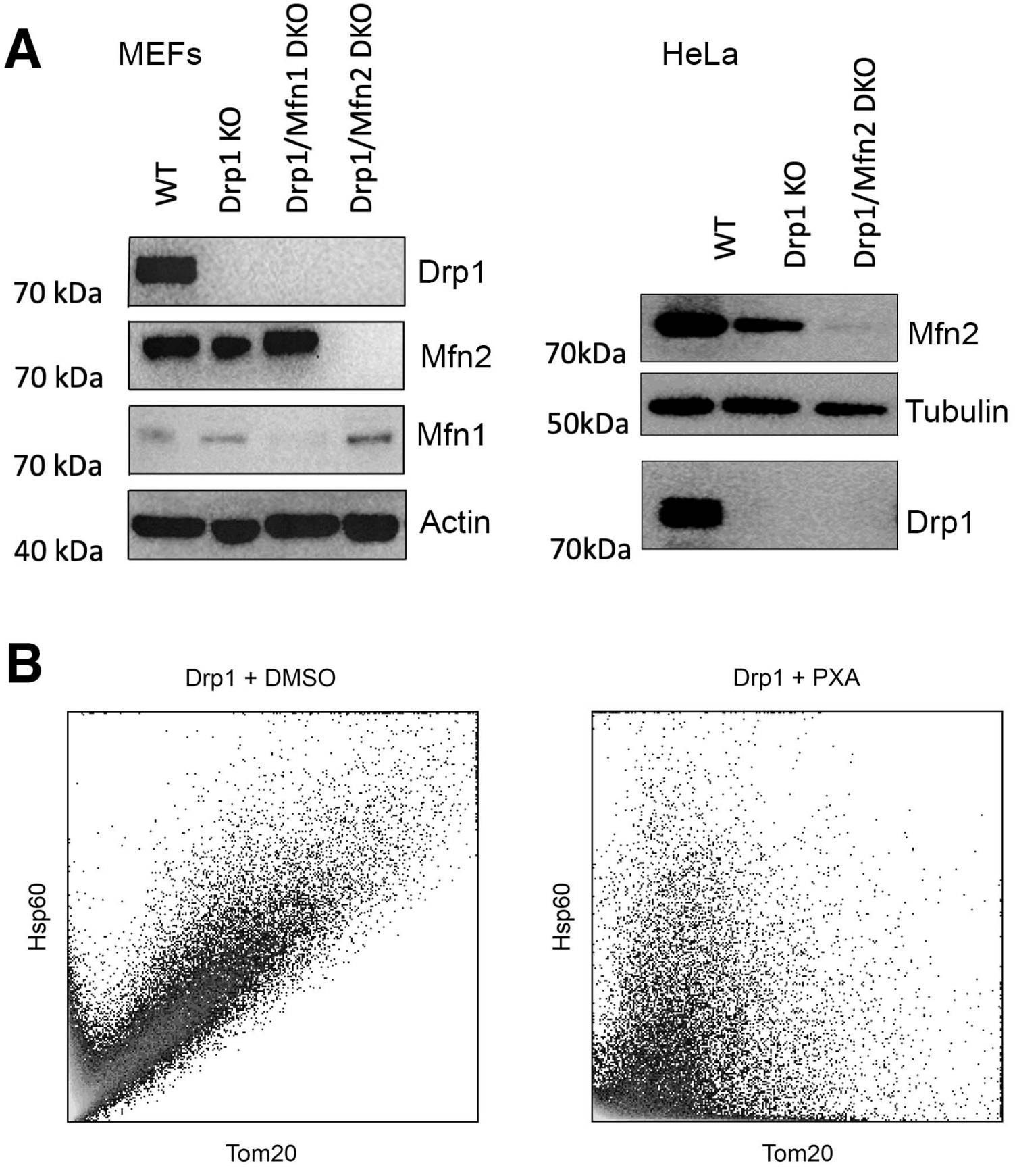
A
MEFs
WT
Drp1 KO
Drp1/Mfn1 DKO
Drp1/Mfn2 DKO
70 kDa
Drp1
70 kDa
Mfn2
70 kDa
Mfn1
40 kDa
Actin
HeLa
WT
Drp1 KO
Drp1/Mfn2 DKO
70kDa
Mfn2
50kDa
Tubulin
70kDa
Drp1
B
Drp1 + DMSO
Drp1 + PXA
Hsp60
Tom20
Hsp60
Tom20

Fig. S1

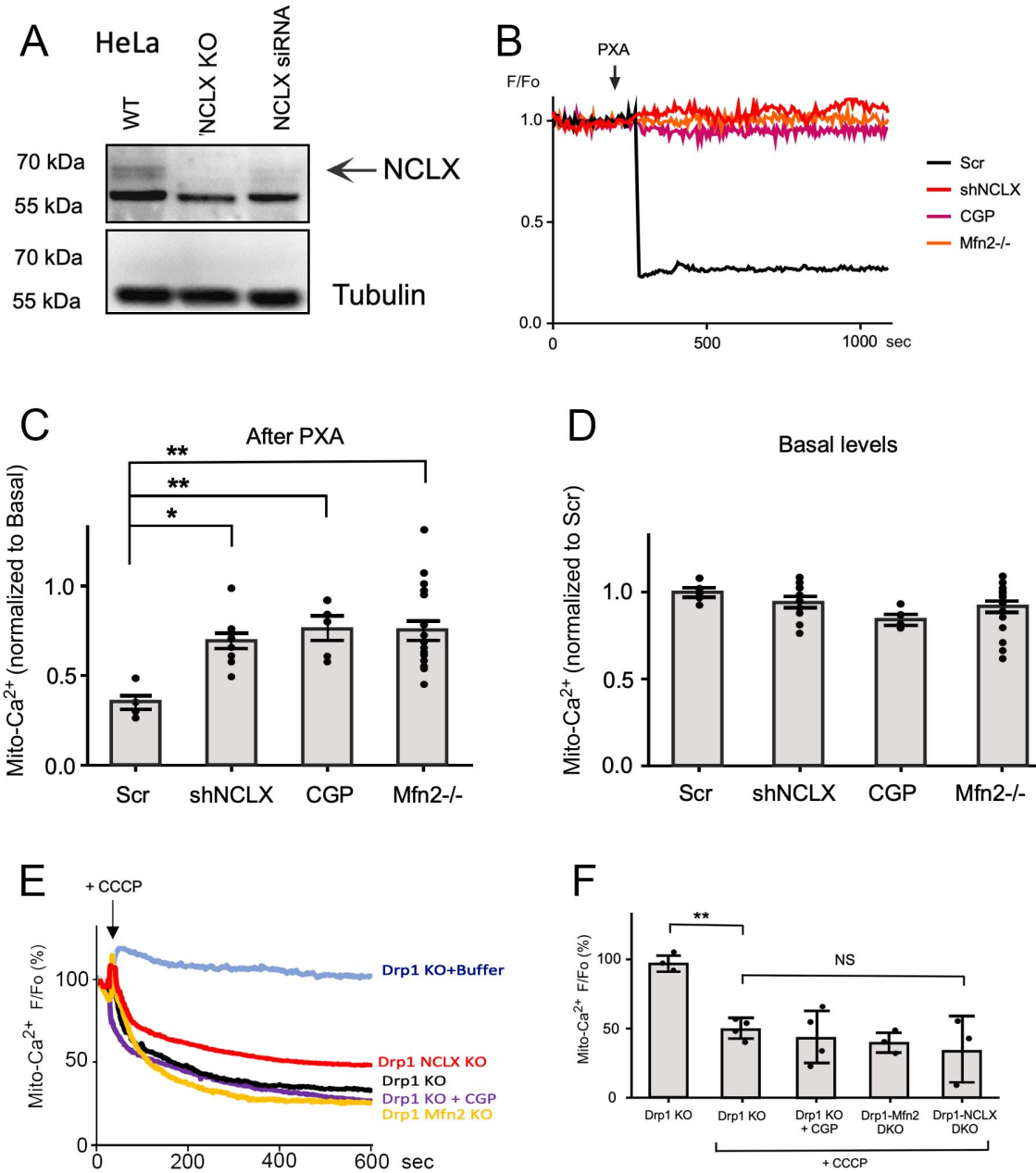
A
HeLa
WT
NCLX KO
NCLX siRNA
70 kDa
55 kDa
NCLX
70 kDa
55 kDa
Tubulin
B
PXA
F/Fo
1.0
0.5
0.0
0
500
1000 sec
Scr
shNCLX
CGP
Mfn2-/-
C
After PXA
**
**
*
Mito-Ca2+ (normalized to Basal)
1.0
0.5
0.0
Scr
shNCLX
CGP
Mfn2-/-
D
Basal levels
Mito-Ca2+ (normalized to Scr)
1.0
0.5
0.0
Scr
shNCLX
CGP
Mfn2-/-
E
+ CCCP
Mito-Ca2+ F/Fo (%)
100
50
0
0
200
400
600 sec
Drp1 KO+Buffer
Drp1 NCLX KO
Drp1 KO
Drp1 KO + CGP
Drp1 Mfn2 KO
F
**
NS
Mito-Ca2+ F/Fo (%)
100
50
0
Drp1 KO
Drp1 KO
Drp1 KO + CGP
Drp1-Mfn2 DKO
Drp1-NCLX DKO
+ CCCP

Fig. S2

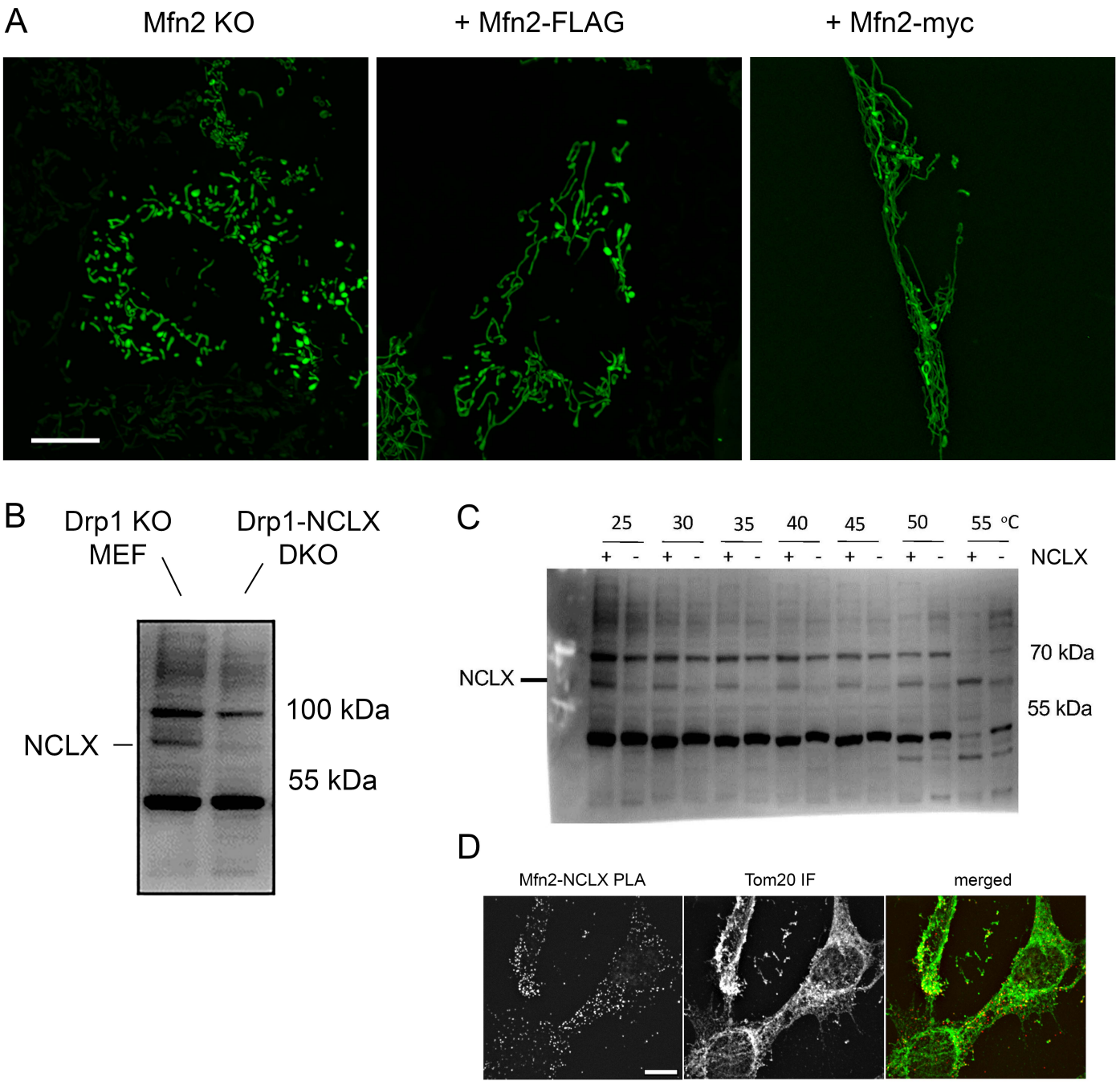
A
Mfn2 KO
+ Mfn2-FLAG
+ Mfn2-myc
B
Drp1 KO MEF
Drp1-NCLX DKO
NCLX
100 kDa
55 kDa
C
25 30 35 40 45 50 55 °C
+ - + - + - + - + - + - + - NCLX
NCLX
70 kDa
55 kDa
D
Mfn2-NCLX PLA
Tom20 IF
merged

Fig. S3

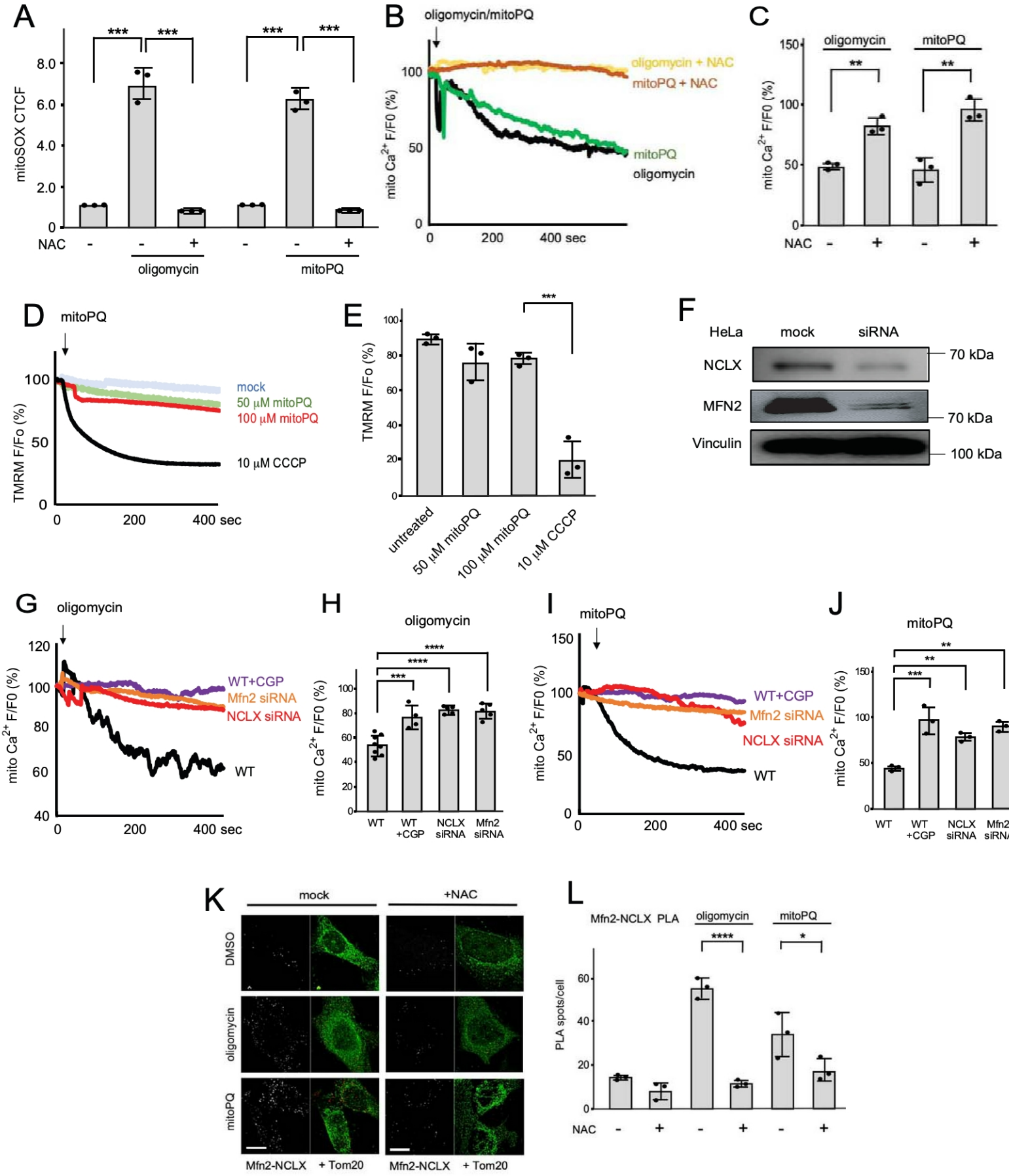

Fig. S4

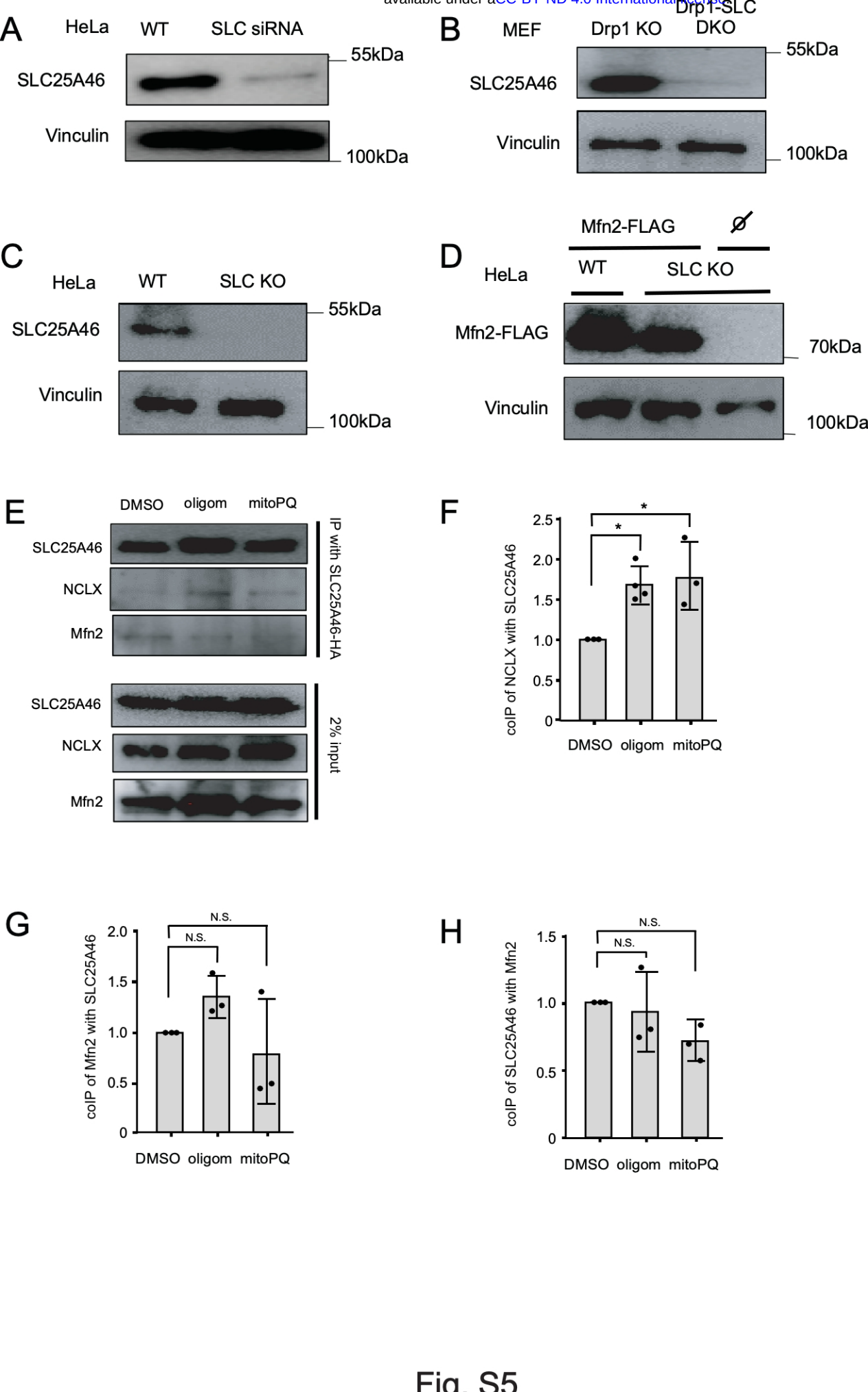

Fig. S5

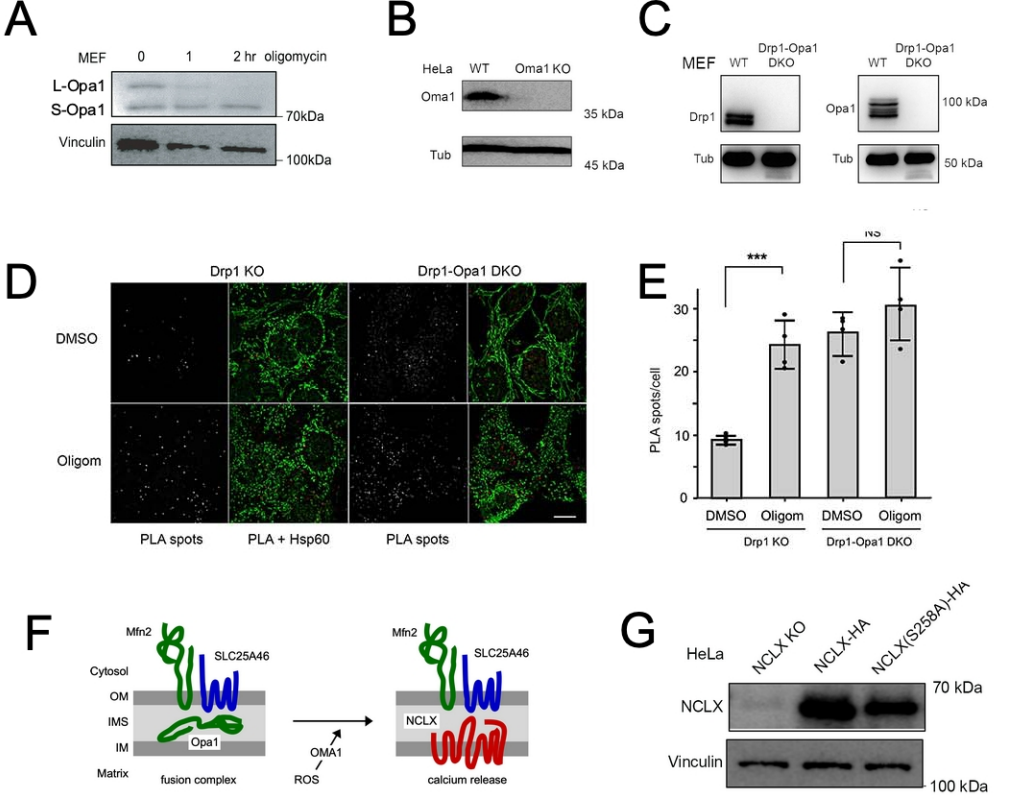
A
MEF 0 1 2 hr oligomycin
L-Opa1
S-Opa1
70kDa
Vinculin
100kDa
B
HeLa WT Oma1 KO
Oma1
35 kDa
Tub
45 kDa
C
MEF
Drp1-Opa1 DKO
WT
Drp1
Tub
Opa1
100 kDa
50 kDa
D
Drp1 KO
Drp1-Opa1 DKO
DMSO
Oligom
PLA spots
PLA + Hsp60
PLA spots
E
***
NS
PLA spots/cell
DMSO
Oligom
Drp1 KO
Drp1-Opa1 DKO
F
Mfn2
SLC25A46
Cytosol
OM
IMS
IM
Opa1
Matrix
fusion complex
OMA1
ROS
NCLX
calcium release
G
HeLa
NCLX KO
NCLX-HA
NCLX(S258A)-HA
NCLX
70 kDa
Vinculin
100 kDa

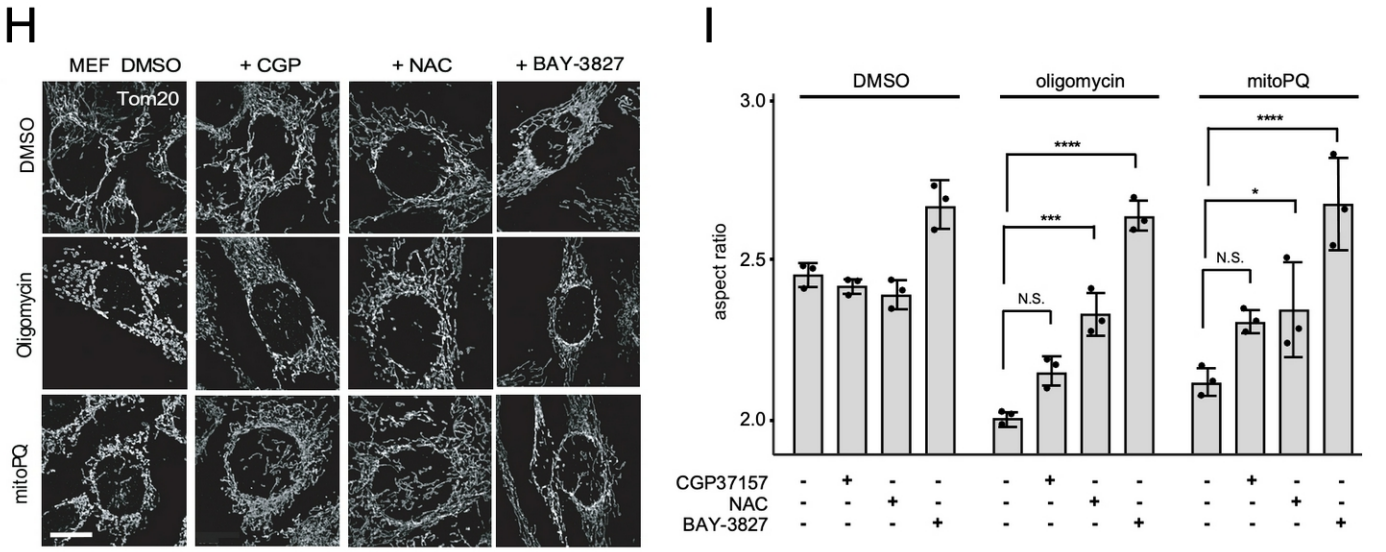
H
MEF DMSO
+ CGP
+ NAC
+ BAY-3827
Tom20
DMSO
Oligomycin
mitoPQ
I
DMSO
oligomycin
mitoPQ
aspect ratio
3.0
2.5
2.0
****
***
*
N.S.
CGP37157
NAC
BAY-3827

Fig. S6

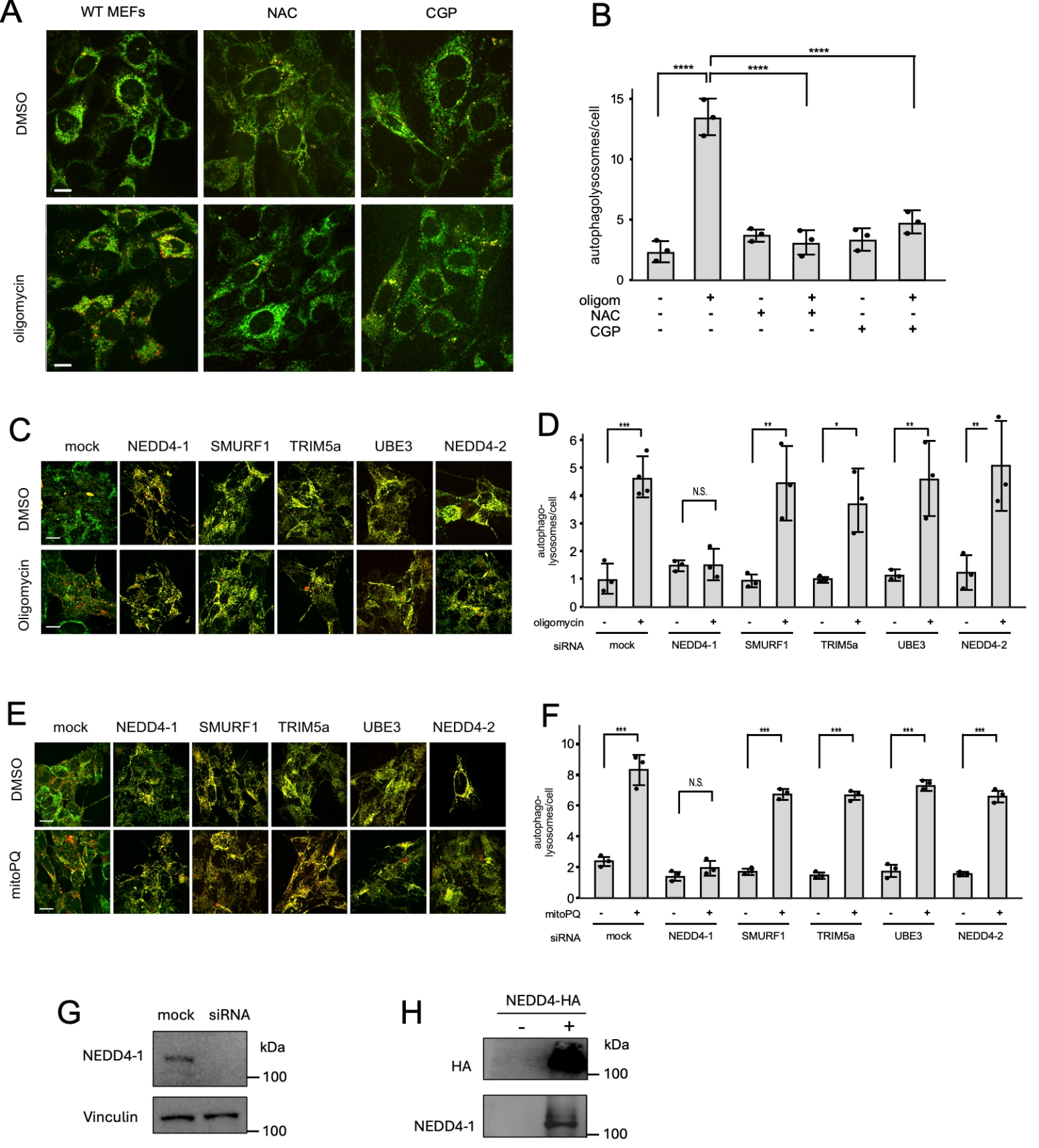
A
WT MEFs
NAC
CGP
DMSO
oligomycin
B
autophagolysosomes/cell
****
****
****
oligom
NAC
CGP
C
mock
NEDD4-1
SMURF1
TRIM5a
UBE3
NEDD4-2
DMSO
Oligomycin
D
autophago-lysosomes/cell
***
N.S.
**
*
**
**
oligomycin
siRNA
mock
NEDD4-1
SMURF1
TRIM5a
UBE3
NEDD4-2
E
mock
NEDD4-1
SMURF1
TRIM5a
UBE3
NEDD4-2
DMSO
mitoPQ
F
autophago-lysosomes/cell
***
N.S.
mitoPQ
siRNA
mock
NEDD4-1
SMURF1
TRIM5a
UBE3
NEDD4-2
G
mock
siRNA
NEDD4-1
kDa
100
Vinculin
100
H
NEDD4-HA
HA
kDa
100
NEDD4-1
100

Fig. S7